

An imaging line survey of OMC-1 to OMC-3

Averaged spectra of template regions

N. Brinkmann¹, F. Wyrowski¹, J. Kauffmann², D. Colombo¹, K.M. Menten¹, X. D. Tang^{1,3,4}, and R. Güsten¹

¹ Max-Planck-Institut für Radioastronomie, Auf dem Hügel 69, D-53121 Bonn, Germany
e-mail: brinkmann@mpi.fr-bonn.mpg.de

² Haystack Observatory, Massachusetts Institute of Technology, Westford, MA 01886

³ Xinjiang Astronomical Observatory, Chinese Academy of Sciences, 830011 Urumqi, PR China

⁴ Key Laboratory of Radio Astronomy, Chinese Academy of Sciences, 830011 Urumqi, PR China

Received: ; Accepted:

ABSTRACT

Context. Recently, sensitive wide-bandwidth receivers in the millimetre regime have enabled us to combine large spatial and spectral coverage for observations of molecular clouds. The resulting capability to map the distributions of lines from many molecules simultaneously yields unbiased coverage of the various environments within star-forming regions.

Aims. Our aim is to identify the dominant molecular cooling lines and characteristic emission features in the 1.3 mm window of distinct regions in the northern part of the Orion A molecular cloud. By defining and analysing template regions, we also intend to help with the interpretation of observations from more distant sources which cannot be easily spatially resolved.

Methods. We analyse an imaging line survey covering the area of OMC-1 to OMC-3 from 200.2 to 281.8 GHz obtained with the PI230 receiver at the APEX telescope. Masks are used to define regions with distinct properties (e.g. column density or temperature ranges) from which we obtain averaged spectra. Lines of 29 molecular species (55 isotopologues) are fitted for each region to obtain the respective total intensity.

Results. We find that strong sources like Orion KL have a clear impact on the emission on larger scales. Although not spatially extended, their line emission contributes substantially to spectra averaged over large regions. Conversely, the emission signatures of dense, cold regions like OMC-2 and OMC-3 (e.g. enhanced N_2H^+ emission and low HCN/HNC ratio) seem to be difficult to pick up on larger scales, where they are eclipsed by signatures of stronger sources. In all regions, HCO^+ appears to contribute between 3% and 6% to the total intensity, the most stable value for all bright species. N_2H^+ shows the strongest correlation with column density, but not with typical high-density tracers like HCN, HCO^+ , H_2CO , or HNC. Common line ratios associated with UV illumination, CN/HNC and CN/ HCO^+ , show ambiguous results on larger scales, suggesting that the identification of UV illuminated material may be more challenging. The HCN/HNC ratio may be related to temperature over varying scales.

Key words. ISM: clouds – ISM: molecules – ISM: individual objects: Orion A – Submillimeter: ISM – Methods: observational

1. Introduction

The northern part of the Orion A molecular cloud is one of the most prominent regions of current low- to intermediate-mass star formation, whose close proximity of just ~ 400 pc (Menten et al. 2007; Kounkel 2017) enables us to spatially resolve its physically and chemically different regions. Continuum maps show substructures which divide Orion A into morphologically different regions: the bright OMC-1 in the south, with a group of filaments radiating away from its central region (O’Dell et al. 2008 and references therein, e.g. Wiseman & Ho 1998), and the less prominent OMC-2/3 in the north.

OMC-1 hosts star formation and is heavily influenced by intense UV radiation from the young massive Trapezium stars. In addition to the Trapezium, Orion BN/KL (hereafter KL) and Orion South are sites of recent star formation (O’Dell et al. 2008). Their positions are indicated in Fig. 2. OMC-1 also includes an archetypical photon-dominated region (PDR), the Orion Bar, outflows, and the eponymous hot core (e.g. Masson et al. 1984) containing a rich chemistry of complex molecules, but also more quiescent gas around it. OMC-2 and OMC-3, located northwards of OMC-1, appear to be a continuation of the

gas in OMC-1, apart from a shift in velocity (e.g. O’Dell et al. 2008; Peterson & Megeath 2008). A large number of pre-stellar Class 0 and Class I objects following the filamentary structure have been discovered through submillimetre observations (e.g. Chini et al. 1997; Johnstone & Bally 1999; Lis et al. 1998), in addition to a number of brown dwarfs (Peterson et al. 2008). In contrast to OMC-1, there are no massive O/B stars, resulting in very different conditions with outflows driven by young embedded stars (Peterson & Megeath 2008 and references therein, e.g. Yu et al. 1997), but without strong UV radiation.

Investigating the characteristics of these distinct regions helps us to understand how low- to high-mass star formation influences the surrounding material and vice versa. Previous line surveys could be biased in that they have often been focused on a single or few positions (e.g. Sutton et al. 1985; Blake et al. 1987; Tercero et al. 2010, 2011; Esplugues et al. 2013; Johnstone et al. 2003), or spatially extended regions were mapped in selected molecular lines only (e.g. Ungerechts et al. 1997), missing out on information a complete frequency coverage offers.

New opportunities arise with sensitive, wide-bandwidth receivers which combine an extensive frequency coverage with a mapping speed sufficient for large fields of view. This enables us

now to obtain a comprehensive and unbiased picture of a molecular cloud. It facilitates the deduction of a variety of physical and chemical conditions using several molecular tracers. These possibilities start being utilised in lower frequency regimes (Pety et al. 2017 and companion papers, e.g. Gratier et al. 2017; Bron et al. 2018 focusing on Orion B or the LEGO project started with Kauffmann et al. 2017). Our data set described in Section 2 deals with higher energies, and is thus sensitive to higher critical densities and constitutes a useful complement to these observations.

This will help us to better understand the conditions (e.g. column density, temperature, strength of UV illumination) under which different molecules are excited, and in particular identify those molecules predominantly present in very specific environments (e.g. N_2H^+ in dense cores; see also Pety et al. 2017). This information is crucial for understanding emission of more distant molecular clouds, including extragalactic sources.

Although CO emission is dominant in the 1.3 mm window, its share of the total intensity (and thus cooling) changes for distinct regions (see also Goldsmith 2001). Comparing the influence of different molecular species to the cooling in Orion A under various conditions will help us to develop templates. These can be used to ‘reproduce’ spectra of other clouds when regions with different physical and chemical conditions are not resolved.

2. Observations and data reduction

2.1. Observations

All observations were carried out with the Atacama Pathfinder Experiment (APEX) 12 m submillimetre telescope (Güsten et al. 2006) using the PI230 receiver operating in the 1.3 mm atmospheric window. We covered the area of OMC-1 to OMC-3 from 200.2 to 281.8 GHz with data collected over several observing periods from October 2015 to November 2018.

The PI230 receiver offers 32 GHz bandwidth per tuning, apportioned into two sidebands and two polarisations, with the two polarisation mixers co-aligned on sky. Eight Fourier Transform Spectrometer (FFTS4G) backends each provide 65536 channels for 4 GHz. An overlap of 0.2 GHz between two backends results in 7.8 GHz coverage for each sideband and polarisation per tuning. The sideband rejection is ≈ 20 dB. The width of the telescope beam changes from around $22''$ to $31''$ over the 1.3 mm window.

The overall spatial coverage of around $400'' \times 1900''$, corresponding to roughly 0.8×3.8 pc at the distance of the Orion Nebula Cluster, was achieved with on-the-fly maps scanned in the x - and y -directions in steps of $8''$ with a dump time of 0.3 seconds. The reference position was $\alpha_{2000} = 5^{\text{h}}31^{\text{m}}14.5^{\text{s}}$, $\delta_{2000} = -5^{\circ}52'29.0''$. The frequency coverage was obtained with 12 overlapping frequency set-ups as shown in Fig. 1. The mean and median system temperatures in main-beam brightness temperature scale (T_{mb}) determined over all observations are $T_{\text{sys}}^{\text{mean}} \approx 266$ K and $T_{\text{sys}}^{\text{median}} \approx 239$ K, respectively. Mean and median receiver temperatures were $T_{\text{rec}}^{\text{mean}} \approx 81$ K and $T_{\text{rec}}^{\text{median}} \approx 78$ K, respectively.

2.2. Calibration and data reduction

All data reduction was done with the GILDAS¹ software package. This included analysis of spectra and maps of the lines’ intensity distribution. In the first processing step the data were calibrated and correction factors for the beam efficiencies applied

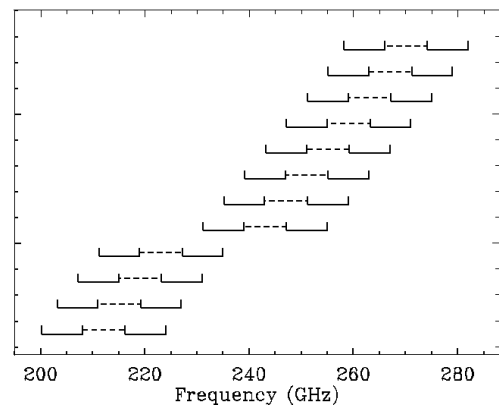


Fig. 1: Twelve overlapping frequency set-ups were used to cover the 1.3 mm window, each providing 2×7.8 GHz bandwidth.

Table 1: Main beam efficiencies (η_{mb}^0) and surface accuracy (σ) used to correct the data from different observing periods

Observing period	η_{mb}^0	σ [μm]
October 2015 - December 2015	0.62	30
July 2016 - November 2016	0.73	30
April 2017	0.74	30
July 2017	0.66	30
May 2018 - July 2018	0.73	15
November 2018	0.75	13

separately for each observing period. These correction factors were obtained from Jupiter continuum pointings at different frequencies. The observed peak temperature of the planet was compared to the expected value calculated by the GILDAS ASTRO module, yielding the main beam efficiency. These main beam efficiencies were then fitted by the Ruze formula, facilitating a frequency dependent correction for every observing period, summarised in Table 1. The exact value of the surface accuracy of the dish has only a marginal impact on the data observed in the 1.3 mm window, however. The main beam efficiency varies by $\lesssim 5\%$ over the observed frequency range. The spectra are also converted from corrected antenna temperature, T_{A}^* , to T_{mb} units in this step, which is thus the temperature scale used in this paper.

A substantial amount of data was collected during the commissioning phase of the PI230 receiver, entailing larger uncertainties. However, parts of the maps have been observed repeatedly in different observing periods such that efficiency corrected spectra could be compared and the earlier data validated, suggesting our calibration uncertainty to be around 30% overall.

In the next processing step we removed spikes, artefacts, and spurious lines that only appeared during the early commissioning of the receiver/backend system and affect parts of the data. Furthermore, spectra with $T_{\text{sys}} \geq 600$ K were rejected. While single channel spikes are readily identified by simple scripts, the artefacts needed to be manually identified and blanked as they showed continuous behaviour towards their edges, making it more challenging to discriminate between them and unaffected channels. A larger number of spectra were checked for each backend and each frequency setting for the different observing days.

¹ <http://www.iram.fr/IRAMFR/GILDAS>

To identify and remove spurious lines, we did a first assignment of all observed lines to molecular transitions from the JPL² (Pickett et al. 1998) and CDMS³ (Endres et al. 2016) molecular spectroscopy databases using the WEEDS (Maret et al. 2011) extension for GILDAS. If a line could not be identified, we checked if it was present in all relevant backends and frequency settings. The respective channels in the originating backends were blanked if the line only appeared in some instances.

2.3. Final data set

In the following processing step, a first-order baseline was subtracted from each spectrum. The boundaries of the line windows were based on the Orion KL spectrum, where we expect the broadest lines and strongest overlap between them. To simplify the analysis and speed up both imaging and the extraction of spectra, we assembled all data for each backend and each frequency set-up and gridded it using the same template cube with a smoothed beam size of 32". This results in 96 data cubes (8 backends \times 12 frequency set-ups), each containing around 3000 spectra and each of which with 65536 channels (corresponding to a resolution of 0.07 – 0.09 kms⁻¹ or 61 kHz). These spectra are intensity corrected, (mostly) artefact-free, baseline subtracted, and arranged on the same grid, and form the basis for all further analyses.

The 1.3 mm window gives us access to a variety of molecular species and transitions. In this paper we want to concentrate on 29 species (55 isotopologues), which are listed in Table 2. We can work with our data set both in terms of imaging and spectral analysis. An example of the differing spatial extensions of typical molecular tracers is given in the integrated intensity maps of Fig. 2. The maps are resampled to a resolution of 0.4 km s⁻¹, resulting in a typical rms noise of around 0.5 K. However, not all species contained in our data set can be mapped as for an individual image pixel their intensity may be too low. Those molecules (like CF⁺) are detectable when we average over larger areas. These averaged spectra will be further described in Sections 3.2 and 3.3.

3. Analysis

The final data set offers a starting point for varied analyses. In this paper, we want to concentrate on the cooling by different molecular species depending on their environment, focusing on an observational point of view.

3.1. Ancillary data

Attributing column density, temperature, or the strength of UV irradiation to different parts of Orion A is done with the help of ancillary data. Dust column density⁴ and temperature based on *Herschel* data are from Guzmán et al. (2015), while C65 α emission data (here used to define the dense PDR region) are from Wyrowski et al. (1997). Dust and gas temperature are expected to be coupled for densities $\sim 3 \times 10^4$ cm⁻³ (Galli et al. 2002), and Guzmán et al. (2015) found that for the examined MALT90 clumps (Jackson et al. 2013; Foster et al. 2013, 2011) under 22 K ammonia and dust temperatures agree within ± 3 K,

² <http://spec.jpl.nasa.gov/>

³ <http://www.astro.uni-koeln.de/cdms/>

⁴ Converted from g cm⁻² to cm⁻² under the simplifying assumption that all mass comes from H₂, $1\text{g} \approx 2.134 \times 10^{23}$ molecules.

Table 2: All considered species and isotopologues.

species	isotopologues
CO	CO, ¹³ CO, C ¹⁸ O, C ¹⁷ O, ¹³ C ¹⁸ O
c – C ₃ H ₂	c – C ₃ H ₂
C ₂ H	C ₂ H, C ₂ D
CF ⁺	CF ⁺
CH ₃ CCH	CH ₃ CCH
CH ₃ CN	CH ₃ CN
CH ₃ OH	CH ₃ OH
CN	CN, ¹³ CN
CS	CS, ¹³ CS, C ³⁴ S, C ³³ S
HCCCN	HCCCN
HCN	HCN, DCN, H ¹³ CN, HC ¹⁵ N
HCO	HCO
HCO ⁺	HCO ⁺ , DCO ⁺ , H ¹³ CO ⁺ , HC ¹⁸ O ⁺ , HC ¹⁷ O ⁺
HCS ⁺	HCS ⁺
HDO	HDO
H ₂ CCO	H ₂ CCO
H ₂ CO	H ₂ CO, HDCO, H ₂ ¹³ CO
H ₂ CS	H ₂ CS, HDCS, H ₂ C ³⁴ S
H ₂ S	H ₂ S
HNC	HNC, DNC, HN ¹³ C
HNCO	HNCO
N ₂ H ⁺	N ₂ H ⁺ , N ₂ D ⁺
NO	NO
NS	NS
OCS	OCS
SiO	SiO, ²⁹ SiO, ³⁰ SiO
SO	SO, ³⁴ SO
SO ⁺	SO ⁺
SO ₂	SO ₂

Notes. Summary of the species and isotopologues used for our analysis. A List of all transitions is found in Sect. A.1

while the uncertainties become larger with increasing temperature. We will mainly use the temperature map to differentiate between colder (< 25 K) and warmer (≥ 25 K) regions. Maps of gas kinetic temperatures based on NH₃ (Orion A) and H₂CO (OMC-1 only) observations can be found in Friesen et al. (2017) and Tang et al. (2018), respectively. As the utilised molecular lines require higher column densities to be excited, these maps do not cover all of the ambient material within our maps. Hence we decided on the use of dust-derived temperatures. Reproductions of the column density and dust temperature maps (reprojected using our template data cube) are shown in Fig. 3.

3.2. Regions and masks

Masks were used to define regions meeting certain conditions (e.g. column density or temperature ranges). These masks were mostly based on dust column density and temperature maps, but in some cases also selected around chosen coordinates. To this end, the maps were reprojected using the same template cube as for the gridding of our observational data, such that combinations of masks (e.g. high column density concurrent with low temperature) were possible. See Table 3 for a summary of the selected regions and their basic properties. For a better visual idea of the spatial extension of these regions, images of the masks are included in the Appendix (Fig. B.1).

Our choice of masks aims to assess the effects of temperature and column density, for example. For the reasons described in Section 3.3, KL and Orion South are excluded in some masks, despite matching the column density or temperature criteria. We have masks with only one condition ('high column density' vs. 'low column density', 'high temperature without KL and Orion

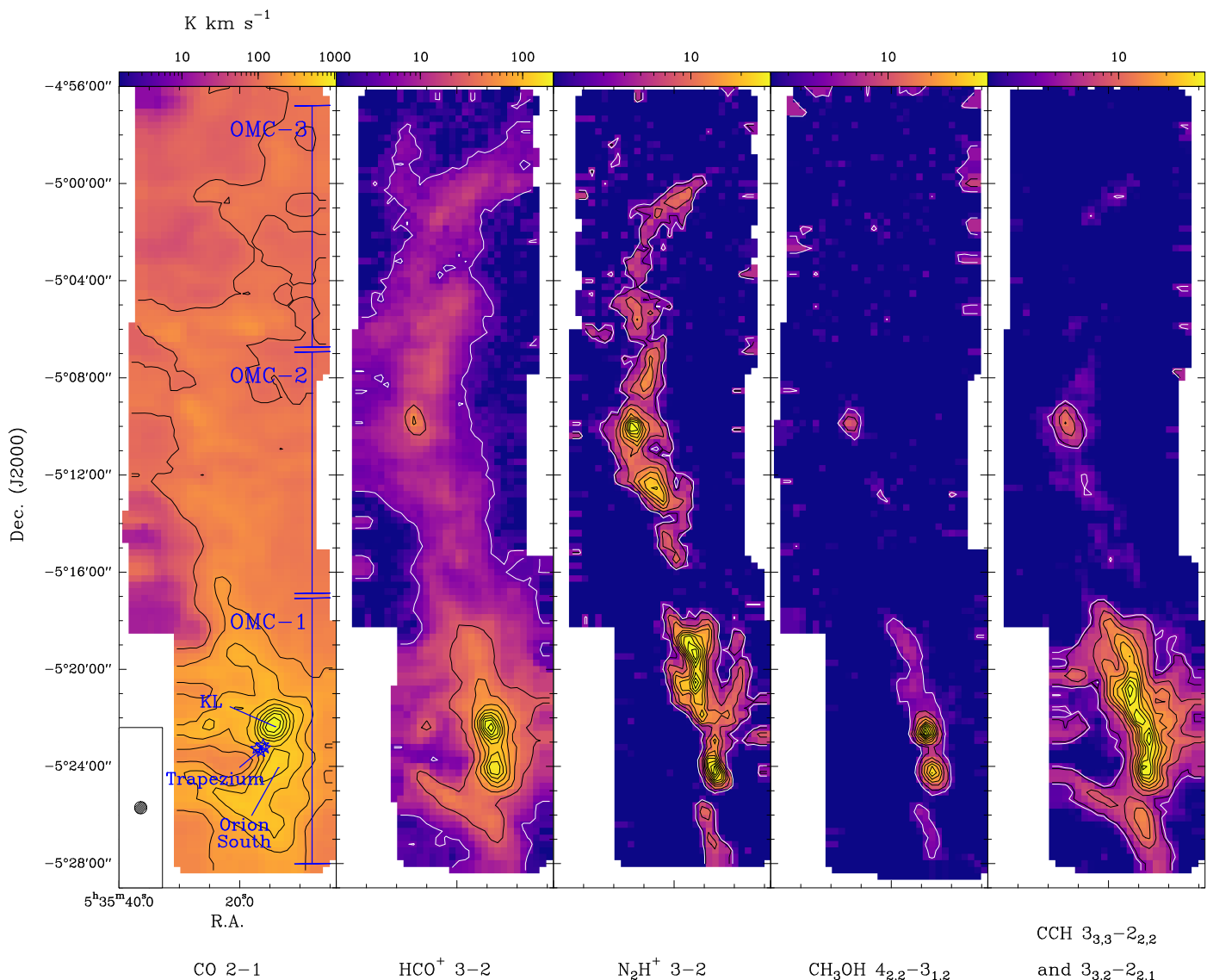


Fig. 2: Selected integrated intensity $[5,15] \text{ km s}^{-1}$ maps. Black contours run from 10% to 90% of the maximum value in steps of 10%, while the white contour shows the 3σ level. The maps highlight some of the molecules typically used as tracers: CO for the bulk of molecular gas, HCO^+ as an indicator of high density, N_2H^+ for cold dense gas, CH_3OH for shocked material, and C_2H associated with UV irradiation. The velocity range used for the maps does not encompass the whole line width (which differs strongly, especially comparing OMC-1 to OMC-3), but covers all central velocities.

South’ vs. ‘low temperature’), but also more restrictive masks, which also define other parameters (‘high column density, low temperature’ vs. ‘low column density, low temperature’ vs. ‘low column density, high temperature’ vs. ‘high column density, high temperature without KL and Orion South’). The masks ‘high column density’ and ‘high column density without KL and Orion South’ intend to show how the spatially quite compact emission of KL and Orion South influences the larger scale emission. Additionally, UV irradiation is considered in the masks ‘ H II ’ and ‘dense PDR’. Choosing this ‘dense PDR’ traced by radio recombination lines, instead of a more ‘diffuse PDR’ traced by C II (Pabst et al. 2019), has the advantage of the edge-on view in Orion. This means we will only probe the actual PDR and are not affected by projection effects. Earlier papers (Turner & Thaddeus 1977) pointed out that the ‘radical region’ may be a chemically distinct environment within OMC-1, although subsequent observations were not conclusive (Greaves & White 1992). We

decided to include this region in our analysis, hoping that our unbiased data set might advance its characterisation. Column density and temperature values listed in Table 3 for the ‘radical region’ are thus not its defining features. Lastly, using no mask at all (‘all averaged’) and employing the results from the other regions, we can evaluate which features or regions dominate on the largest considered scale and which might disappear, indicating that those latter regions may be hard to identify in other, spatially unresolved sources.

The exact values we chose for the column density and temperature thresholds ($N = 3.6 \times 10^{22} \text{ cm}^{-2}$, $T = 25 \text{ K}$) are somewhat arbitrary. We selected them such that they divide Orion A broadly into the denser parts of the filament ($N \geq 3.6 \times 10^{22} \text{ cm}^{-2}$) and the ambient material ($N < 3.6 \times 10^{22} \text{ cm}^{-2}$), and distinguish between the historically established regions OMC-1 ($T > 25 \text{ K}$) and OMC-2/3 ($T < 25 \text{ K}$). Based on these basic dis-

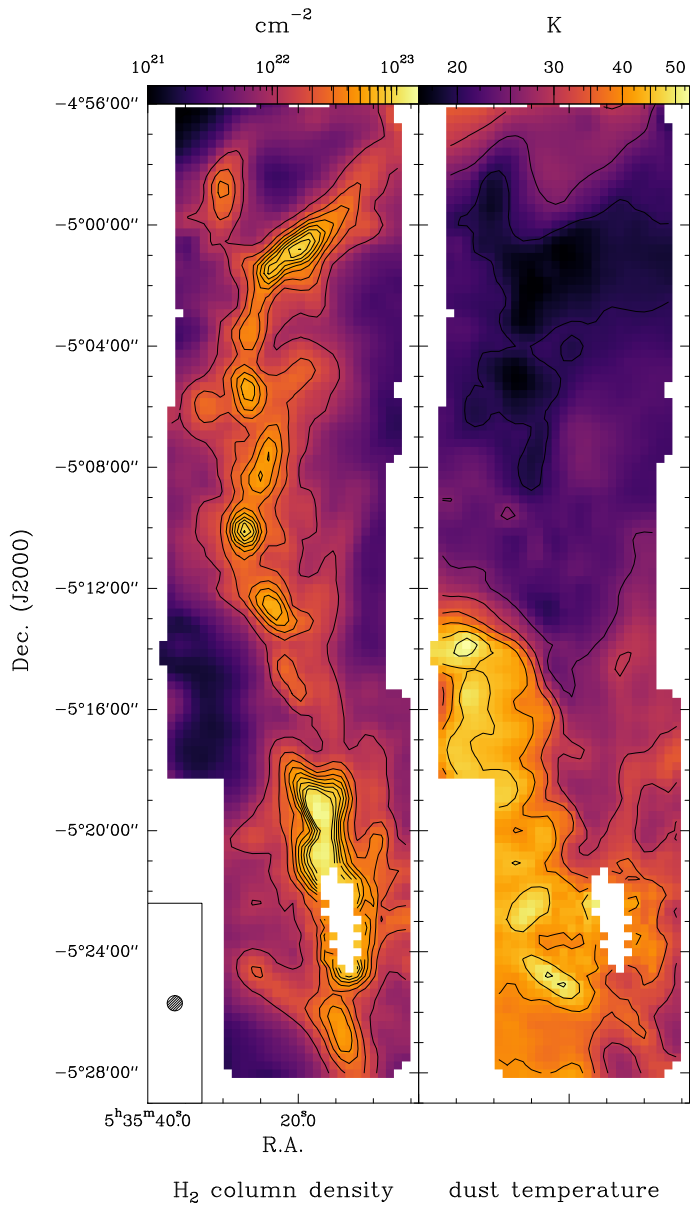


Fig. 3: Dust derived column density and temperature map, modified (reprojected and cropped, the column density unit converted) from Guzmán et al. (2015). The area around KL and Orion South is saturated and blanked.

tinctions, combinations of masks are added and complemented by the ‘H II’, ‘dense PDR’ and ‘radical region’ masks.

Our masks are thus not devised to divide Orion A into strictly disjointed regions, but to explore the emission of template regions meeting physical or chemical conditions. A listing of all overlaps between the selected regions is given in Table A.3.

Table 3: Selected regions and their fundamental properties.

region	explicit mask	approx. size [arcmin ²]	column density range [cm ⁻²]	median column density [cm ⁻²]	temperature range [K]	median temperature [K]	label ^(†)
all averaged	no mask	210.0	$9.3 \times 10^{20} - > 1.4 \times 10^{23}$ (*)	1.0×10^{22} (*)	17 - 53 (*)	25 (*)	1
high column density	$N \geq 3.6 \times 10^{22}$ cm ⁻²	23.3	$3.6 \times 10^{22} - > 1.4 \times 10^{23}$ (*)	4.9×10^{22} (*)	17 - 51 (*)	27 (*)	2
high column density without KL and Orion South	$N \geq 3.6 \times 10^{22}$ cm ⁻²	21.5	$3.6 \times 10^{22} - 1.4 \times 10^{23}$	4.9×10^{22}	17 - 51	27	3
high column density, low temperature	$N \geq 3.6 \times 10^{22}$ cm ⁻² $T < 25$ K	9.2	$3.6 \times 10^{22} - 9.3 \times 10^{22}$	4.7×10^{22}	17 - < 25	19	4
high column density, high temperature, without KL and Orion South	$N \geq 3.6 \times 10^{22}$ cm ⁻² $25 < T < 55$ K	11.5	$3.6 \times 10^{22} - 1.4 \times 10^{23}$	5.5×10^{22}	26 - 51	32	5
low column density	$N < 3.6 \times 10^{22}$ cm ⁻²	186.7	$9.3 \times 10^{20} - < 3.6 \times 10^{22}$	9.0×10^{21}	17 - 53	25	6
low temperature	$T < 25$ K	102.1	$2.1 \times 10^{21} - 9.3 \times 10^{22}$	1.2×10^{22}	17 - < 25	21	7
low column density, low temperature	$N < 3.6 \times 10^{22}$ cm ⁻² $T < 25$ K	92.9	$2.1 \times 10^{21} - < 3.6 \times 10^{22}$	1.1×10^{22}	17 - < 25	22	8
low column density, high temperature	$N < 3.6 \times 10^{22}$ cm ⁻² $25 < T < 55$ K	93.7	$9.3 \times 10^{20} - < 3.6 \times 10^{22}$	7.5×10^{21}	25 - 53	34	9
high temperature, without KL and Orion South	$25 < T < 55$ K	105.2	$9.3 \times 10^{20} - 1.4 \times 10^{23}$	8.5×10^{21}	25 - 53	33	10
H II	high H31 α emission (**)	6.4	$7.9 \times 10^{21} - 6.7 \times 10^{22}$ (*)	1.7×10^{22} (*)	36 - 51 (*)	42	11
radical region (***)	$130'' \times 130''$ around $\alpha_{2000} = 5^h 35^m 16.51^s$ $\delta_{2000} = -5^\circ 19' 33.0''$	5.1	$1.8 \times 10^{22} - 1.4 \times 10^{23}$	5.8×10^{22}	27 - 38	30	12
dense PDR	$N < 3.6 \times 10^{22}$ cm ⁻² high C65 α emission (****)	4.7	$8.8 \times 10^{21} - 3.5 \times 10^{22}$	1.8×10^{22}	37 - 51	44	13

Notes. (†) To be used as an identifier in later plots. (*) The area around Orion KL and Orion South is saturated, thus the given maximum column density, maximum temperature, and median values are actually lower limits. (**) Mask based on an integrated [-20, 15] km s⁻¹ intensity image of the H31 α emission at 210501.788 MHz, where pixels with an integrated intensity over ≈ 3.1 K km s⁻¹ were selected. (***) Coordinates based on Greaves & White (1992). (****) Mask based on an integrated intensity image of the C65 α emission at 23415.9609 MHz from Wyrowski et al. (1997), where pixels with an integrated intensity over 4 K km s⁻¹ were selected.

3.3. Obtaining total intensities

The total intensity of different molecular species for the different regions was determined in three steps. Firstly, the spectrum of the region was extracted from our data cubes using the masks described in section 3.2. All spectra within a mask were combined into a single spectrum, the ‘regional spectrum’ or average. The idea is that local effects should average out in this step when the area is large, while common characteristic features will add up. Smoothing along the frequency axis to a resolution of around 305 kHz was done to improve the signal-to-noise ratio. Three of these averaged spectra are shown as examples in Fig. 4.

In the second step, the spectral lines listed in Table A.1 were considered in Gaussian fits. Line-of-sight velocities do not vary significantly within the mapped area, from $\sim 9 \text{ km s}^{-1}$ for most of OMC-1 (especially when excluding KL and Orion South with slightly lower velocities) and increasing to $\sim 12 \text{ km s}^{-1}$ towards OMC-3. Different velocity components thus overlap in a spectrum. The list of lines is based on the spectrum obtained with the high column density mask (which includes Orion KL and Orion South), where we expect the greatest number of lines. Omitted are complex molecules with the exception of CH_3OH , CH_3CN , and CH_3CCH . The lines of CH_3OCH_3 or CH_3OCHO , for example, are numerous but weak and their contribution to the overall emission as typical hot core molecules should be negligible on larger scales. The main goal is to capture most of the line emission, which in some cases means that not each individual transition is fitted. The automated fitting is more robust when strongly overlapping lines are not fitted separately, but covered in a single Gaussian fit. This favouring of robustness was abandoned when the overlapping lines belonged to different species. In that case, the lines were fitted separately. Overlap between lines becomes an issue whenever KL and Orion South are involved, hence the decision to only include them in two larger regions, as automated fitting is not feasible otherwise.

In the third and final step all lines above 5σ with reasonable widths and velocity were considered to be real detections and the area of their fit added to the total intensity of their respective species.

Noise levels vary within a single spectrum depending on frequency, and between different spectra due to the varied spatial extension of the regions. This influences the possibility to detect very weak lines and will be addressed further in Fig. B.2.

4. Results

The averaged total intensity for each species and region is listed in Table 4, together with the detection limit for each region. Owing to space constraints, the formal fit errors are listed separately in Table A.2, but they usually amount to 2–6% for all species and regions. Due to the overall low noise levels and the high number of free parameters, the fit errors for a single line are very small. The actual uncertainties are thus dominated by the calibration uncertainties discussed in Section 2.2.

The high column density region has the highest averaged total intensity with $\sim 1360 \text{ K km s}^{-1}$. Removing just the region around KL and Orion South has a significant impact on the overall emission and reduces the averaged total intensity by 48%, although the removed area represents only 8% of the high column density region. The regions ‘high column density, high temperature, without KL and Orion South’ and ‘H II’ have comparable averaged total intensities ($\sim 954 \text{ K km s}^{-1}$ and $\sim 925 \text{ K km s}^{-1}$), which are a factor of ~ 3 above average ($\sim 319 \text{ K km s}^{-1}$). The averaged total CO intensity is also similar for these two re-

gions, their differences lying in the species with less emission. The ‘dense PDR’ and ‘radical’ regions both emit a factor of ~ 2 above average, but their share of CO emission differs by around 20%, indicating that their emission profiles (meaning the breakdown of the total emission into contributions from different species) are distinct from each other. The ‘high temperature without KL and Orion South’ region is most similar to the ‘averaged’ region not only in terms of total intensity, but also regarding the most prominent species. The remaining regions, including ‘high column density, low temperature’, emit below average.

For easier comparison, hereafter the data is presented in three complementing ways, each highlighting different aspects. Figure 5 shows the visualisation for the different species with the example of our average data (where no mask was used). The normalised intensity of all species in descending order is shown in Fig. 5a with a logarithmic plot, down to 0.1% of the CO intensity. This order of species is used in the corresponding total intensity plots for all other regions (see Fig. B.2). For the comparison of regions, this representation of the data helps to make shifts in the influence of species more apparent. The pie charts (Fig. 5b and Fig. B.4) visualise the percentage of the total intensity originating from different species, with shares under 2% summed under ‘other’. Plots in this form are more conducive from an observational point of view, as they highlight the most dominant and accessible species.

The third visualisation (Fig. B.3) concentrates more on a comparison between species. The plot again shows the percentage share of each molecule, while the colour bar helps to highlight in which region each species has its largest or smallest share and which species are overall stronger or weaker emitters.

Of the 55 species considered in our analysis, 15 are seen to contribute over 2% each of the total intensity for at least one region. Members of these 15 species account for around 88% to 94% of line emission in the 1.3 mm window in all cases (or 5.6% to 53% when excluding CO and its isotopologues). In addition to CO and ^{13}CO , only HCO^+ and H_2CO are prominent in every region, each contributing between 3% and 6% in all cases.

In terms of averaged total intensity, there is a factor of ~ 8 between the lowest (‘low column density, low temperature’) and highest (‘high column density’) regions. The high column density region has the lowest share of CO and the highest diversity of species noticeably involved in cooling. SO_2 , with a share of 11.4% being the most important coolant after CO in the high column density region, is no longer relevant when KL and Orion South are removed (its share drops to around 1%; see also Fig. B.4a, B.4b and Fig. B.2a, B.2b). SO and CH_3OH show similar trends. In the high column density region, their total intensities exceed that of the typically strong emitters HCN, HCO^+ , and H_2CO , while they lose importance without KL and Orion South.

The regions ‘high column density, low temperature’ and ‘high column density, high temperature, without KL and Orion South’ are parts of ‘high column density without KL and Orion South’ (see also Fig. B.1), coinciding with OMC-2/OMC-3 and OMC-1, respectively. Both in terms of averaged total intensity and as suggested by the pie charts and detailed normalised intensities (Fig. B.4b, B.4c, B.4d and Fig. B.2b, B.2c, B.2d), OMC-1 dominates the emission. Higher N_2H^+ emission, indicative of OMC-2/OMC-3, is not seen in the ‘high column density without KL and Orion South’ region, which is instead very similar to OMC-1 alone.

The regions ‘low column density’, ‘low temperature’, ‘low column density, low temperature’ and ‘low column density, high temperature’ are similar in the sense of high CO shares (60% to 67% for CO, 15% to 21% for ^{13}CO) and only two to four species

over 2% (Fig. B.4e, B.4f, B.4g, and B.4h). Their averaged total intensities are similar and below average. Their distinctions lie in the lower intensity species (Fig. B.2e, B.2f, B.2g, and B.2h).

The regions ‘high temperature, without KL and Orion South’ and ‘dense PDR’ are similar to each other and—with the the exception of SO emission and slightly different CO shares—to the ‘averaged’ region (Fig. B.4i, B.4l, 5b). The averaged total intensity is noticeably higher in the ‘dense PDR’ region than in the two others. The differences between regions lie again in the fainter species (Fig. B.2i, B.2l, 5a).

The ‘H II’ region is the only other region, in addition to ‘high column density’, with relevant SO₂ emission and also has higher shares of CH₃OH and SO, which is the dominant coolant after CO and ¹³CO. The ‘radical region’ has the highest shares of C₂H and CN and is the only other region besides ‘high column density, low temperature’ (dense part of OMC-2/OMC-3) with notable shares of N₂H⁺.

4.1. Approximating the emission of KL and Orion South

While automated fitting procedures are problematic for high column density and high temperature environments with heavily overlapping lines, we can approximate the emission around KL and Orion South from our existing regions. With the known pixel sizes of ‘high column density’ and ‘high column density without KL and Orion South’ we can gauge the emission of the region and compute its average. The result is not as robust as the others, as more lines are expected for some species which are not accounted for in our routine (especially for SO₂, SO, and CH₃OH), and omitted complex organic molecules like CH₃OCH₃ presumably have non-negligible impact here. However, the overall results, as presented in Table 5 and Fig. B.5, are in general agreement with Schilke et al. (1997) for the 325 to 360 GHz frequency regime. The dominant species are in both cases SO₂, followed by CO, SO, CH₃OH, and HCN.

4.2. Correlations and line ratios on large scales

In the following analysis of correlations and line ratios, the integrated intensity for a given species always refers to the sum of all of its considered transitions in the 1.3 mm window listed in Table A.1. For some species (CO, ¹³CO, C¹⁸O, HCO⁺, H¹³CO⁺, HCN, HNC, N₂H⁺, and CS) this involves only one transition, but includes several for others (C₂H, CN, CH₃OH, H₂CO, and SO). For the discussion of line ratios, we use simplified quantum numbers for species with one transition, and mark those species with multiple transitions with the letter Σ. Not all energy levels, for example of CH₃OH, will be populated in all regions, but its integrated intensity still carries meaning as a measure of the cooling in the examined frequency range. Furthermore, neighbouring transitions from complex species like CH₃OH will strongly overlap in the broad lines from extragalactic sources, thus also inherently limiting the transferability of results concerning single or a few transitions only.

Correlations between species do not only point to similarities in their physical and chemical behaviour, but also reduce the number of necessary transitions for gauging the conditions in a molecular cloud. If the emission of two species correlates strongly it is possible, for example, to limit the frequency coverage to one species and save observation time. We limit our analysis to 14 species that are typically used as tracers.

All emission correlates to the first order with column density (see also Fig. 6), which will thus influence the correlation

between species. To reduce this effect in our analysis of the 13 regional spectra, we divided the total intensity for each species and region by the respective median column density for the region (see Table 3). This is not as good as a pixel-by-pixel normalisation, but it is more feasible, especially for SO with its numerous partially overlapping lines. Furthermore, the number of data points is small (13 regions), meaning we do not have enough statistical data for a truly reliable correlation coefficient. However, we mainly hope to distinguish between species with strong correlation and those without correlation. Linear correlations were measured with the Pearson correlation coefficient⁵ and are shown in Fig. 6, while selected plots are presented in Figs. B.6 and B.7. Using our averaged (and therefore unresolved) regional data adds uncertainty for the interpretation compared to a pixel-by-pixel analysis (e.g. the discussed column density value, which is only an approximation for the whole region). On the other hand, our averaged data enables us to include species like SO and CH₃OH even in low column density and low-temperature environments.

4.2.1. Correlations and tracers

We expect chemical effects to influence correlation, and also different optical depths of the species. We do not correct for the latter, as our aim is to stay as close to the data an observer might receive from an unresolved source, where the assumptions needed to correct for optical depth may add additional uncertainty.

Strong correlations (≥ 0.90) are found between the typical high-density tracers HCN, HCO⁺, H₂CO, HNC, CS, but also CN. There is generally little spread between the data points in the correlation plots, for example between H₂CO and HCO⁺ (Fig. B.6a) or H₂CO and HCN (Fig. B.6b), but the ‘H II’ region with its high integrated intensities (after normalisation) constitutes a more isolated data point.

To a lesser degree, correlations are also found between H¹³CO⁺ and the other high-density tracers (Fig. B.6c). However, the integrated intensity of the former is often an order of magnitude smaller than for the latter, making its observation more challenging.

Not only is CN correlated with C₂H, which is often associated with UV irradiation (Nagy et al. 2015 and references therein), but it is also correlated with high-density tracers (e.g. Fig. B.6d, B.6e). Another strong correlation is found between the shock tracers (e.g. Bachiller & Pérez Gutiérrez 1997, Sakai et al. 2012, Nagy et al. 2015 and references therein, e.g. Wakelam et al. 2004) SO and CH₃OH (Fig. B.6f).

For the evaluation of correlations between species and column density in this case we have to factor in that the intensities are not normalised (with the median column density). Hence, it is possible to see two species correlating strongly with column density, but not with each other after normalisation (see C¹⁸O and N₂H⁺). Of all the considered species, N₂H⁺ shows the strongest correlation with the median column density (Fig. B.7a), the outlier being the non-detection ($< 5\sigma$) in the ‘dense PDR’ region, where N₂H⁺ is most likely expected to be destroyed. We also see a strong correlation between C¹⁸O and the median column density (Fig. B.7b), but the data points show a wider spread. When considering slope (and intercept) of the linear fit between species and median column density, we see that N₂H⁺ reacts more sensitively to changes in column density. From the more luminous high-density tracers, HNC may corre-

⁵ Calculated using `scipy.stats.pearsonr` from the SciPy library (Jones et al. 2001-2019) in Python.

Table 4: Averaged total intensities $\int T_{\text{mb}} dv$ [K km s⁻¹] for all regions and species. The detection limit is based on the median line width for each region and assumes a $5\sigma_{\text{median}}$ feature. Real detections below this limit may occur, for example when $\sigma_{\text{local}} < \sigma_{\text{median}}$ or when the line is narrow.

species	all averaged	high column density	high column density without KL and Orion South	high column density, low temperature	high column density, high temperature, without KL and Orion South	low column density	low temperature	low column density, low temperature	low column density, high temperature	high temperature without KL and Orion South	H II	radical region	dense PDR
CO	174.21	393.21	303.48	137.13	405.67	146.64	112.19	110.06	187.64	209.34	431.08	279.67	391.86
¹³ CO	45.19	90.51	81.37	46.54	103.78	39.91	38.91	38.10	41.71	48.31	69.57	81.02	71.17
C ¹⁸ O	5.61	12.82	11.22	9.00	12.78	4.83	6.19	5.86	3.79	4.58	6.41	10.19	4.74
C ¹⁷ O	1.89	4.13	3.82	3.19	3.98	1.62	2.16	2.03	1.19	1.50	2.12	3.46	1.73
¹³ C ¹⁸ O	-	0.15	0.14	0.14	0.15	-	0.11	-	-	-	-	0.16	-
c-C ₃ H ₂	0.34	3.27	2.71	0.36	4.09	-	-	-	0.38	1.02	1.41	3.10	3.83
C ₂ H	6.96	30.33	25.48	7.01	37.11	3.96	2.11	1.65	6.19	9.72	18.66	35.05	13.82
C ₂ D	-	0.77	0.70	0.36	0.86	-	-	-	-	-	-	0.78	-
CF ⁺	0.13	0.25	0.21	-	0.21	0.12	0.11	-	-	-	-	-	-
CH ₃ CCH	0.35	10.06	5.14	0.52	8.18	-	-	-	-	0.36	3.74	5.74	-
CH ₃ CN	-	30.02	1.20	-	1.25	-	-	-	-	1.36	1.73	-	-
CH ₃ OH	4.87	87.74	17.96	4.05	25.79	0.73	0.58	0.43	0.85	1.90	40.63	17.96	0.92
CN	9.26	36.02	26.50	9.33	38.77	5.62	3.29	2.05	4.76	8.38	29.60	35.05	17.98
¹³ CN	-	0.37	0.32	-	0.48	-	-	-	-	-	-	0.32	-
CS	4.86	29.57	18.69	3.27	27.50	2.03	1.09	0.96	3.05	5.88	18.63	16.48	8.96
¹³ CS	0.23	2.47	1.33	-	2.01	-	-	-	-	-	1.80	0.97	0.58
C ³⁴ S	0.50	3.32	2.17	-	3.23	-	-	-	0.27	0.56	2.25	1.75	0.93
C ³³ S	-	0.84	0.44	-	0.74	-	-	-	-	-	0.58	0.38	0.28
HC ₃ N	-	17.21	2.28	-	3.23	-	-	-	-	-	6.57	0.84	0.27
HCN	12.46	70.94	36.67	9.37	49.07	4.38	3.02	2.32	6.45	11.62	50.43	26.35	21.14
DCN	0.34	2.51	1.51	0.35	1.96	-	-	-	-	0.33	1.69	1.09	0.34
H ¹³ CN	0.74	7.43	2.24	0.25	2.73	-	-	-	0.19	0.53	2.47	1.61	0.70
HC ¹⁵ N	-	2.42	0.56	-	0.77	-	-	-	-	-	0.97	0.30	-
HCO	-	0.13	0.15	-	0.54	-	-	-	-	-	-	0.25	0.43
HCO ⁺	13.22	61.37	39.97	14.92	52.21	7.29	6.39	5.59	9.42	14.78	50.30	29.17	27.65
DCO ⁺	0.12	1.06	0.81	0.97	0.64	0.07	0.22	0.15	-	-	-	0.48	-
H ¹³ CO ⁺	0.64	3.31	2.55	1.27	3.09	0.15	0.36	0.27	0.30	0.62	2.11	2.30	0.44
HC ¹⁸ O ⁺	-	0.30	0.21	-	0.28	-	-	-	-	-	0.24	0.23	-
HC ¹⁷ O ⁺	-	-	-	-	-	-	-	-	-	-	-	-	-
HCS ⁺	0.13	1.88	1.44	-	2.15	-	-	-	-	0.37	1.21	1.60	-
HDO	-	0.59	-	-	-	-	-	-	-	-	-	-	-
H ₂ CCO	-	0.81	-	-	-	-	-	-	-	-	-	0.16	-
H ₂ CO	12.10	64.62	41.28	17.95	53.55	6.15	5.75	4.42	7.75	12.51	40.88	36.38	21.44
HDCO	-	2.09	0.35	0.18	0.95	-	-	-	-	-	0.37	0.61	-
H ¹³ CO	-	2.34	0.39	0.15	1.04	-	-	-	-	-	0.71	0.29	-
H ₂ CS	1.54	18.10	10.15	-	16.35	-	-	-	0.32	2.15	10.07	10.97	0.27
HDCS	-	-	-	-	0.30	-	-	-	-	-	-	0.26	-
H ₂ C ³⁴ S	-	-	-	-	-	-	-	-	-	-	-	-	-
H ₂ S	-	2.30	-	-	0.49	-	-	-	-	-	-	-	-
HNC	2.86	14.37	10.25	5.53	12.94	1.56	1.70	1.31	1.74	2.97	7.51	10.66	3.71
DNC	0.08	0.63	0.50	0.53	0.56	-	0.11	-	-	-	-	0.52	-
HN ¹³ C	-	0.58	0.47	0.22	0.64	-	0.06	-	-	-	0.27	0.58	-
HNCO	-	2.44	-	-	0.49	-	-	-	-	-	-	-	-
N ₂ H ⁺	2.40	11.14	10.67	9.75	11.40	1.28	2.37	1.62	0.84	2.05	2.67	13.39	-
N ₂ D ⁺	-	0.19	0.20	0.44	-	-	-	-	-	-	-	-	-
NO	0.10	2.23	1.01	0.44	1.24	0.08	0.25	0.24	-	-	1.07	-	-
NS	-	2.26	1.66	-	2.63	-	-	-	-	-	-	2.66	-
OCS	-	5.05	-	-	-	-	-	-	-	-	1.20	-	-
SiO	2.94	27.77	5.83	-	7.30	-	-	-	-	-	13.93	-	-
²⁹ SiO	-	1.64	-	-	-	-	-	-	-	-	-	-	-
³⁰ SiO	-	-	-	-	-	-	-	-	-	-	-	-	-
SO	11.81	129.66	32.39	2.91	42.62	0.97	0.98	0.77	1.61	4.28	65.82	8.00	9.64
³⁴ SO	-	12.05	-	-	0.85	-	-	-	-	-	1.16	0.09	-
SO ⁺	-	-	-	-	0.59	-	-	-	-	-	-	0.13	0.36
SO ₂	2.65	155.03	4.15	-	6.57	-	-	-	-	-	35.27	-	-
sum :	~ 319	~ 1360	~ 711	~ 286	~ 954	~ 227	~ 188	~ 178	~ 279	~ 345	~ 925	~ 641	~ 603
approx. detection limit [K km s ⁻¹] :	0.17	0.29	0.22	0.16	0.20	0.15	0.11	0.10	0.19	0.16	0.38	0.14	0.27

Table 5: Approximated averaged total intensities from the region around KL and Orion South

species	$\int T_{\text{mb}} dv$ [K km s ⁻¹]
CO	1464.9
¹³ CO	199.6
C ¹⁸ O	31.9
C ¹⁷ O	7.8
¹³ C ¹⁸ O	0.3
c-C ₃ H ₂	9.9
C ₂ H	88.2
C ₂ D	1.5
CF ⁺	0.7
CH ₃ CCH	68.9
CH ₃ CN	374.2
CH ₃ OH	921.1
CN	149.8
¹³ CN	1.0
CS	159.4
¹³ CS	16.1
C ³⁴ S	17.0
C ³³ S	5.7
HC ₃ N	195.5
HCN	480.3
DCN	14.5
H ¹³ CN	69.5
HC ¹⁵ N	24.6
HCO	-
HCO ⁺	317.0
DCO ⁺	4.1
H ¹³ CO ⁺	12.4
HC ¹⁸ O ⁺	1.4
HC ¹⁷ O ⁺	-
HCS ⁺	7.0
HDO	7.7
H ₂ CCO	10.4
H ₂ CO	343.3
HDCO	22.9
H ₂ ¹³ CO	25.6
H ₂ CS	113.1
HDCS	-
H ₂ C ³⁴ S	-
H ₂ S	29.8
HNC	63.6
DNC	2.1
HN ¹³ C	2.0
HNCO	31.6
N ₂ H ⁺	16.7
N ₂ D ⁺	0.1
NO	16.7
NS	9.3
OCS	65.3
SiO	289.8
²⁹ SiO	21.2
³⁰ SiO	-
SO	1291.6
³⁴ SO	156.0
SO ⁺	-
SO ₂	1957.2
total	9120.2

late the most with the median column density, in agreement with Pety et al. (2017).

CO and its isotopologues do not show clear correlations with other species (but they do with each other). This may be explained to some degree by optical depth effects, meaning that CO mainly traces the surface of the cloud, while other species probe deeper layers. Especially for C¹⁸O, which is unlikely to be optically thick, depletion may be an important factor. High-density tracers generally profit from higher (volume) densities,

while C¹⁸O may freeze out in these environments if the temperatures are low (as the chance to collide with and stick to dust grains is increased). N₂H⁺ only correlates with the median column density.

4.2.2. Line ratios

A related important diagnostic, especially for extragalactic observations, but also for molecular clouds in the Milky Way, are line or integrated intensity ratios. They are more reliable tracers of physical or chemical conditions than lines from a single species as calibration errors can cancel out for ratios, depending on the observation technique. These ratios can also be examined with our data.

We will examine some integrated intensity ratios which have also been discussed in Pety et al. (2017), Gratier et al. (2017), or Bron et al. (2018), among others, in the 3 mm window. The considered transitions are thus different, but general trends (e.g. HCN/HNC value increasing with temperature) may still be seen with our data. Selected integrated intensity ratios are compiled in Fig. 7.

Our sample supports the notion from Pety et al. (2017) that the CN/HCN ratio is not a reliable tracer of UV illuminated gas. As the photodissociation of HCN produces CN, one might expect the highest ratio in the ‘dense PDR’ region of our data (CN(Σ)/HCN(3 – 2) \approx 0.9). Instead we find it in the ‘low column density’ and ‘radical region’ environments (both \approx 1.3). The lowest ratio is found for the ‘high column density’ region (\approx 0.5). The CN(1–0)/HCO⁺(1–0) ratio, discussed in Bron et al. (2018), is suggested to help distinguish UV-illuminated gas from shielded gas, with higher values associated with higher illumination. We find the lowest value (CN(2 – 1)/HCO⁺(3 – 2) \approx 0.4) for our ‘low column density, low temperature’ region, the highest (\approx 1.2) in the ‘radical region’, not with the expected ‘dense PDR’ (\approx 0.7). So at least on our examined large scales and without correction for optical depth, using this ratio in the 1.3 mm window to trace UV illumination seems difficult too.

The ratio HCN/HNC should increase with temperature (Pety et al. 2017 and references therein, e.g. Graninger et al. 2014) due to HNC reacting with H to form HCN at temperatures \geq 30 K. Indeed we find the three lowest values (HCN(3 – 2)/HNC(3 – 2) = 1.7 – 1.8) for our regions associated with the lowest median temperatures, while the highest two values of 5.7 – 6.7 coincide with the highest temperatures, found in our case in the ‘H II’ and ‘dense PDR’ regions. Larger deviations from this trend are found for the ‘radical region’, for example (see also Fig. B.7c).

In their PCA of Orion B data in the 3 mm window, Gratier et al. (2017) found that a higher N₂H⁺(J = 1 – 0, F1 = 2 – 1, F = 3 – 2,)/CH₃OH(J = 2 – 1, K = 0 – 0, A⁺) ratio possibly highlights the chemistry of the densest cores. This cannot be meaningfully examined for the 1.3 mm window with our spatially unresolved data, and we do not see a correlation with column density. While the emission of both species is higher in regions of enhanced column density in our data, their ratio is not. The highest ratios are not found in the regions encompassing the dense filament, but instead in the ‘low temperature’ and ‘low column density, low temperature’ regions (N₂H⁺(3 – 2)/CH₃OH(Σ) \approx 3.8 – 4.1), while the spectra from the high column density regions have notably lower values (\approx 0.1 for the ‘high column density’, \approx 2.4 for the ‘high column density, low temperature’, and \approx 0.4 for the ‘high column density, high temperature, without KL and Orion South’ region). However, we see a potential correlation of N₂H⁺(3 – 2)/CH₃OH(Σ) with temperature (Fig. B.7d).

4.2.3. Line luminosities

For the interpretation of emission from unresolved and/or extragalactic sources, information on line luminosities [$\text{K km s}^{-1} \text{pc}^2$] is important. Regions with low overall emission may still contribute considerably to the emission of some species if these regions are spatially extended. Conversely, strong but compact emission may be diluted on larger scales. Figure 8 lists the total luminosity (sum over all considered species in the 1.3 mm window) and the values for selected species for all our examined regions, including the approximations for KL and Orion South (see also Section 4.1).

Despite its overall lower emission, the extended ‘low column density’ region is the source of $\sim 75\%$ of the CO, ^{13}CO , and C^{18}O emission, while $\sim 25\%$ can be allotted to the ‘high column density’ region. For the high-density tracers HCO^+ and HNC, but also N_2H^+ , the allocation between low and high column density is around 50%/50%. For HCN and CS it is less of an even split between the two column density regimes and $\sim 65\%$ originate from the high column density region.

A lot of the emission from the high column density region can be attributed to the environment of KL and Orion South: with a size of $< 1\%$ of the total examined area, it emits $\sim 20\%$ of the HCO^+ and HNC, and $\sim 30\%$ of HCN and CS. When considering all emission in the 1.3 mm window, KL and Orion South are the source of roughly 25%.

5. Discussion

By averaging over the area, we highlight the individual emission profile of the regional spectra, including lower intensity species, while ignoring their actual spatial extent (which here mainly influences the respective noise level). This approach might help to characterise sources for which the spatial resolution is not good enough to differentiate between distinct regions. It is also a different approach compared to the analysis of the Orion B data set (Pety et al. 2017; Gratier et al. 2017; Bron et al. 2018) in the 3 mm window, where the focus is more on selected, typically more luminous transitions, not necessarily on a complete inventory of species. We discuss our findings further in this section and compare them with results from other authors.

We find that temperature has a significant impact on the total intensities of our selected regions; considering column density alone is not sufficient. This is illustrated most obviously in the cases of the ‘high column density, low temperature’ and ‘H II’ regions. The former has higher column densities but low overall emission, while the latter has lower median column density but a factor of ≈ 2.6 higher total intensity (total intensity summed over all considered species). We mostly consider temperatures and column densities, but it also seems instructive to keep the main feedback processes in different regions in mind. While the column densities in OMC-2/3 are similar to values found in parts of OMC-1, the energy input in the former is mainly driven by outflows from low-mass protostars, while in the latter it is shared between outflows and feedback from the H II region, as discussed in Berné et al. (2014) and inferred from CO and ^{13}CO 2 – 1 emission. The kinetic energy in KL was found to be dominated by feedback of massive protostars (outflows, jets, explosive motion). In contrast, the Bar exhibits very little outflow activity; its kinetic energy is mainly caused by the expanding H II region.

We find very similar total CO intensities for the ‘high column density’ and ‘dense PDR’ regions ($\sim 393 \text{ K km s}^{-1}$ and $\sim 392 \text{ K km s}^{-1}$), but their total intensities summed over all species vary by more than 50% ($\sim 1360 \text{ K km s}^{-1}$ and $\sim 603 \text{ K km s}^{-1}$).

While the different column densities and temperatures in the two regions still result in similar CO intensities, other species react very differently and are much more enhanced in the ‘high column density’ region. This might again be partly due to opacity effects and CO only tracing the outer layers.

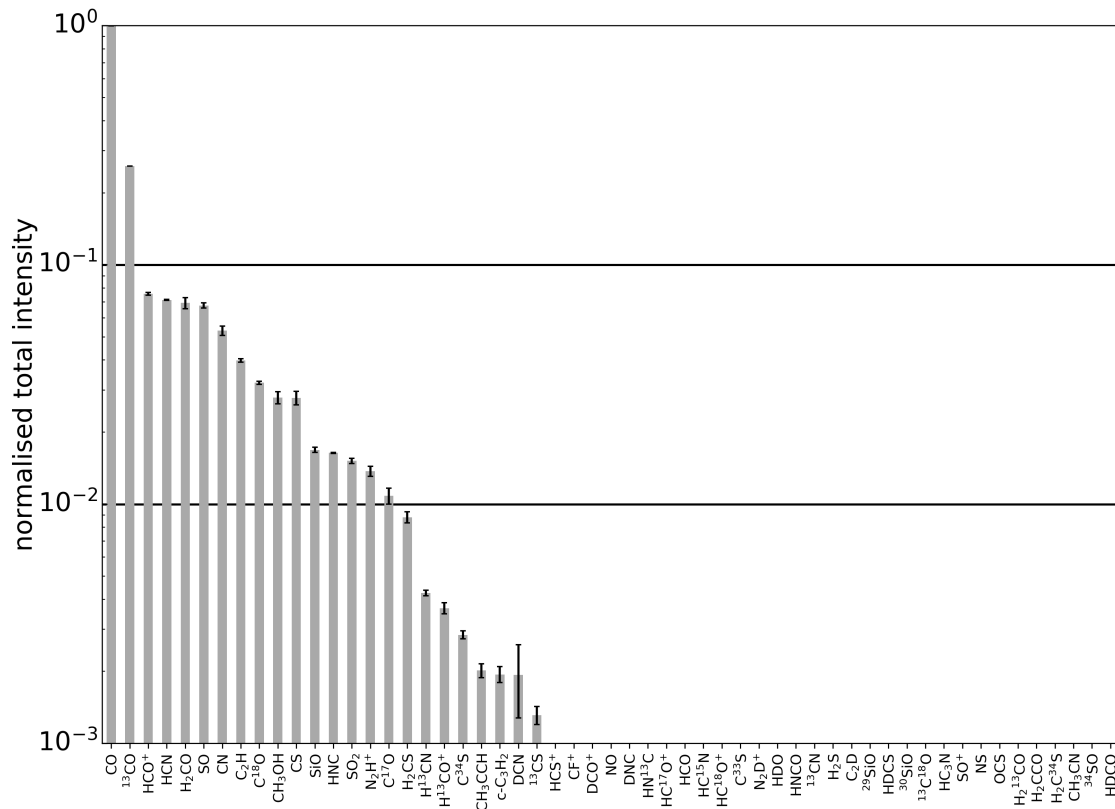
The median column densities for the ‘dense PDR’ and ‘H II’ regions are about a factor of 3 lower than for ‘high column density’ and ‘high column density, high temperature without KL and Orion South’, but their median temperatures are the highest for all considered regions. This might explain their high emission despite overall lower column densities.

5.1. Correlations

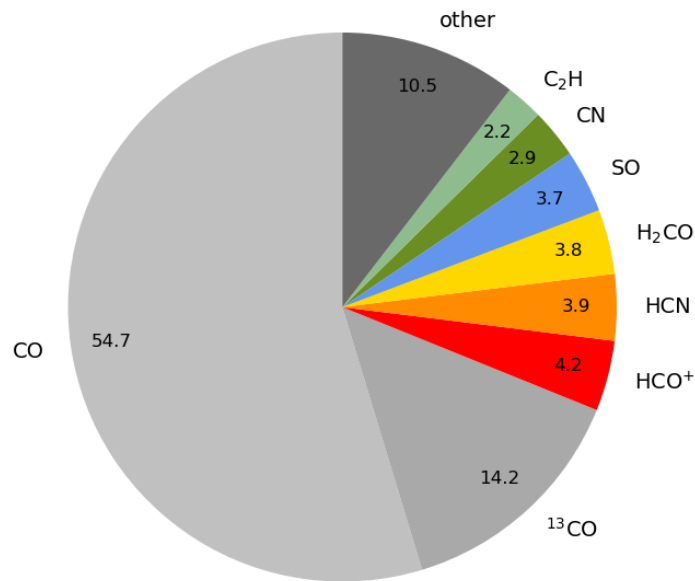
For the further examined most luminous species, strong correlations are typically found between high-density tracers, excluding N_2H^+ . This may be related to the optical depth effects mentioned before, but also to the influence of temperature, as shown in the case of the warm ‘dense PDR’ region, where N_2H^+ does not emit over 5σ despite enhanced column densities. N_2H^+ shows no correlation with any other prevalent species in the 1.3 mm window, but instead with column density. If N_2H^+ data is not available, HNC might overall be a better tracer of column density than HCN or HCO^+ , for example. HNC shows similar intensities to N_2H^+ , however, so it should not be a question of observation time. That HCN does not exclusively trace dense gas was also shown in Kauffmann et al. (2017) for the 1 – 0 transition in Orion A, where HCN was found to trace lower densities $\sim 10^3 \text{ cm}^{-3}$ in cold sections of the cloud. Additionally, they found that the cold dense gas emits too little HCN to explain the luminosities observed in extragalactic sources. This is consistent with the below average emission we see for the OMC-2/3 region in our data (‘high column density, low temperature’).

Different papers discuss additional mechanisms which may excite ‘dense gas’ tracers. As elaborated in Goldsmith & Kauffmann (2017), electron excitation may be important for high-dipole moment molecules in regions where the fraction of ionised carbon is significant. The low-J transitions of HCN (but also HCO^+ , CN, and CS) could thus be observed in lower density environments and may not qualify as indicators of high density. Another mechanism could be radiative trapping (Shirley 2015; Pety et al. 2017). It is argued that fundamental lines of HCN, HNC, and HCO^+ could be excited in regions well below their critical density as the latter is computed assuming optically thin emission only. Both mechanisms could explain our observations. Particularly in OMC-1, where C^+ is abundant (Pabst et al. 2019), the emission of HCN, for example, may originate in part from electron excitation. Additionally, some transitions may have a high optical depth, increasing contributions from photon-trapping. An alternative approach to the detection of low-lying rotational lines is discussed in Liszt & Pety (2016). They discuss the observability of transitions for HCO^+ , HNC, and CS in regions where the density is far below the critical density. The authors find, in the limit of weak collisional excitation, that there is a column density (not a volume density) that will produce a given output.

We find that the typical UV tracers CN and C_2H correlate not only with each other, but also strongly with high-density tracers. This means that tracing UV illumination on large scales could be challenging, as enhanced CN or C_2H emission might not necessarily be indicative of higher UV illumination.



(a) all averaged normalised total intensities



(b) all averaged pie chart

Fig. 5: Normalised total intensity and pie chart for our averaged data. The order of species in the normalised plot is also used for every other region (see Fig. B.2). The pie chart gives the percentage of the total intensity originating from different species. Shares under 2% are summed under ‘other’.

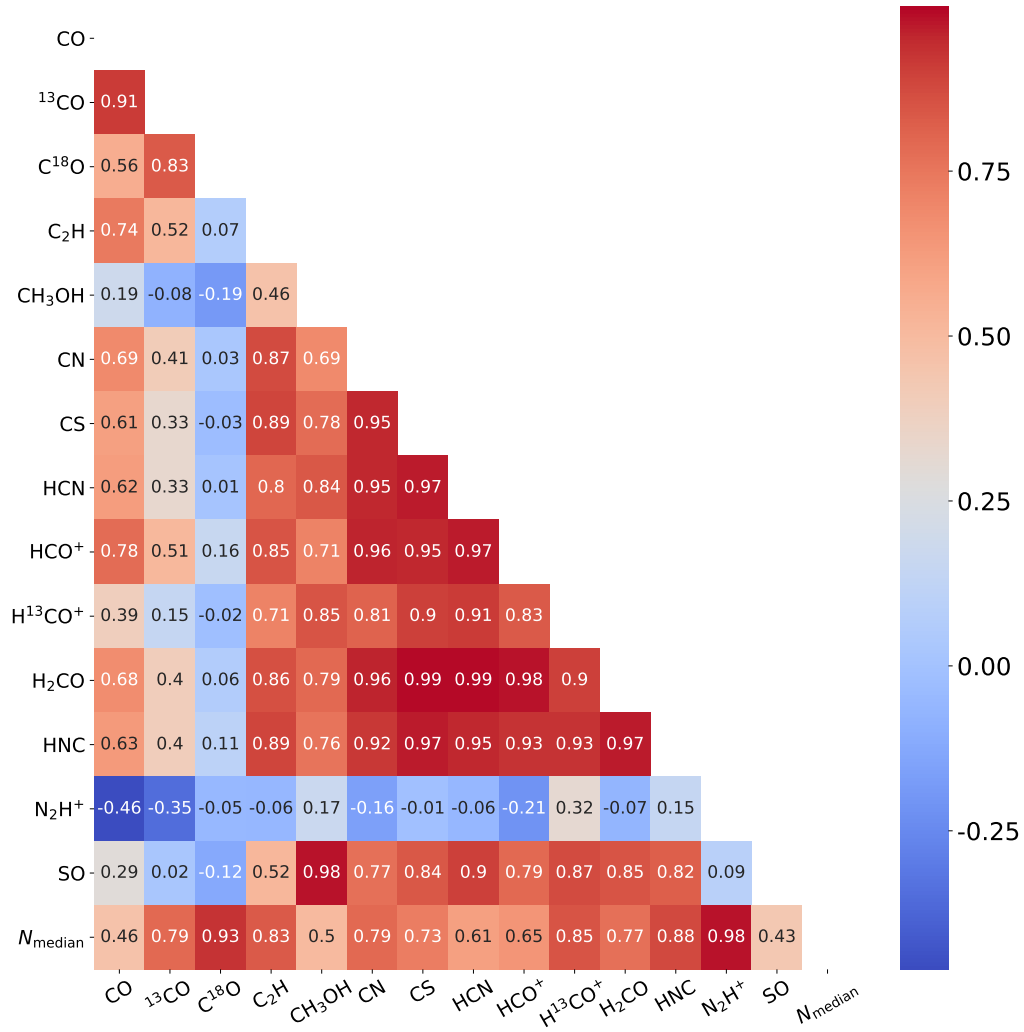


Fig. 6: Pearson product-moment correlation coefficients between prevalent species (normalised with the median column density) and between prevalent species and the median column density.

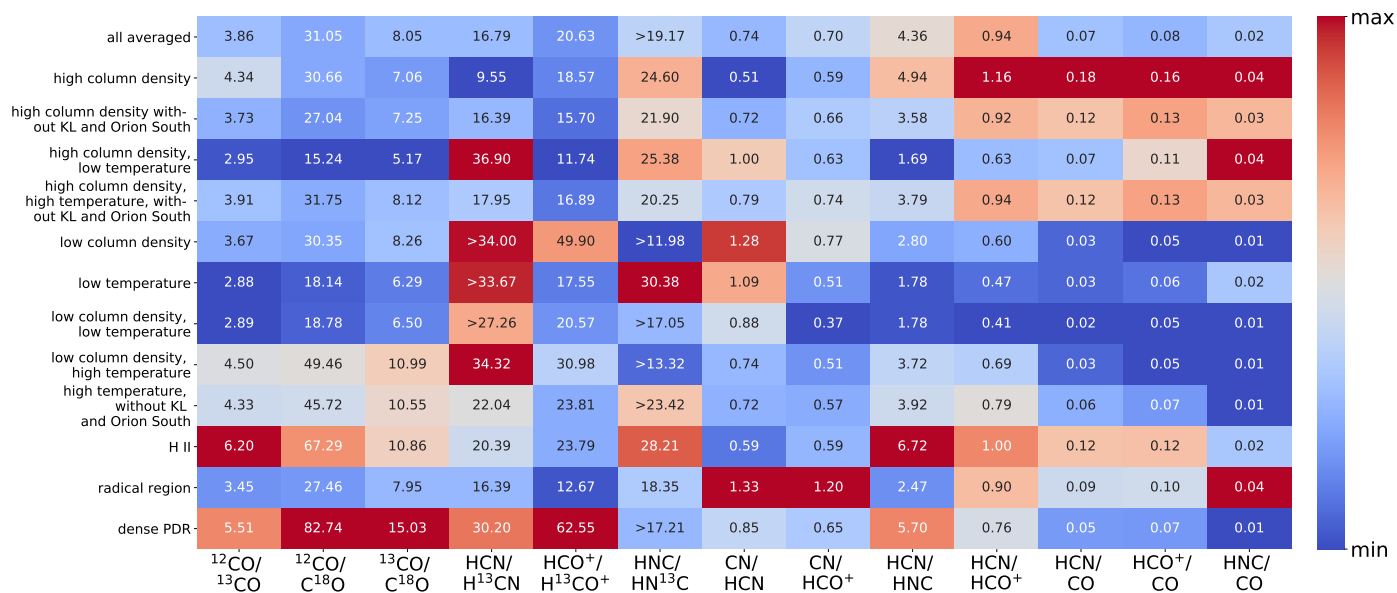


Fig. 7: Integrated intensity ratios of selected species for the different regions. Lower limits are based on a hypothetical line with the median line width for the respective region and a peak intensity of five times the local noise level. Assuming an uncertainty of 30% for the intensities, all ratios have an uncertainty of $\sim 42\%$. The maximum and minimum value of the colour bar are not defined globally, but for every ratio (column) individually.

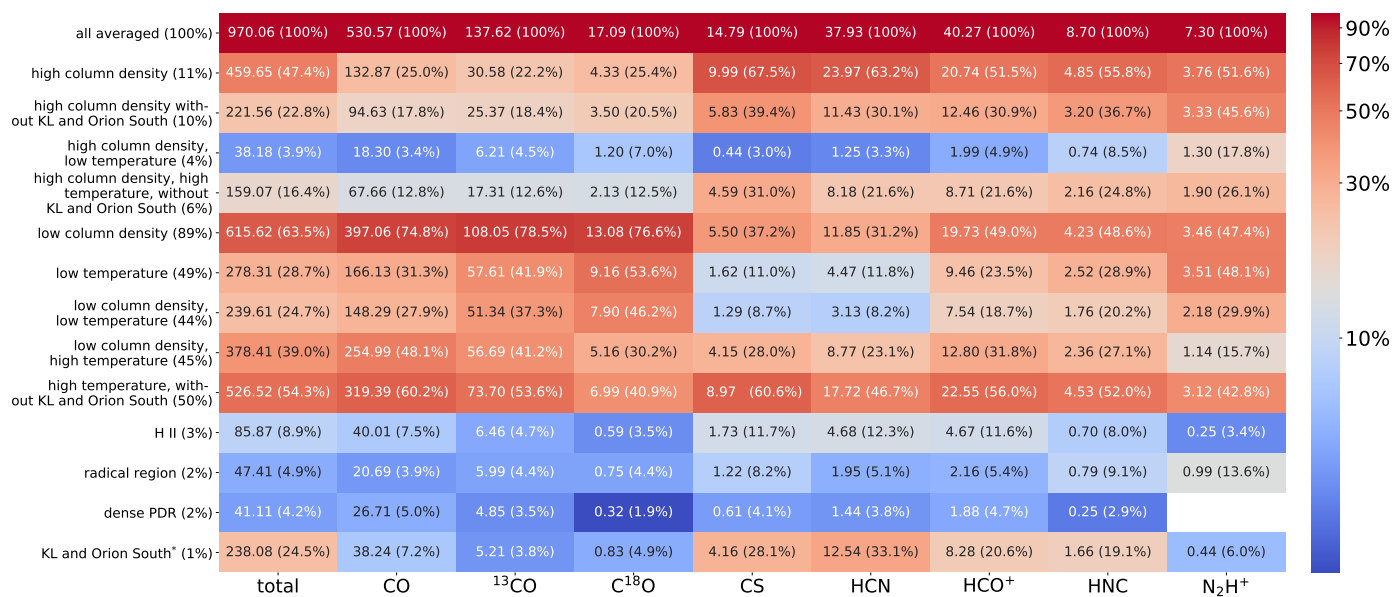


Fig. 8: Total line luminosity (first column) and absolute and relative line luminosities [$\text{K km s}^{-1}\text{pc}^2$] for selected species in the different regions. A region's relative size is given in the brackets beside its name. Regions are generally not disjointed, but overlap to varying degrees. Additionally, rounding uncertainties for both intensities and region sizes accumulate and slightly different detection limits apply for each region. Hence the percentages do not add up to 100% and should be considered as estimates. (*) Approximated as described in Section 4.1.

5.2. Emission on larger scales

The stark difference in the emission profile of KL and Orion South (see Section 4.1) compared to the other regions was also found for some species in Ungerechts et al. (1997), where the integrated intensity maps of SO or HC₃N showed distributions strongly peaked towards KL. While we find that line emission from KL and Orion South has a noticeable impact on spectra averaged over larger scales (compare Fig. B.4a and B.4b, but also appreciate that SiO and SO₂ are detectable in the averaged spectrum despite not being detected for the majority of regions), this influence of high column density regions on the averaged spectrum was not seen by Watanabe et al. (2017) for the spectrum of W51 in the 3 mm window. Their spatial coverage of 39 pc×39 pc is significantly larger than for our data set, so emission from high-density regions is expected to be smeared out more, such that they find a dominance of the quiescent material over the averaged spectrum.

In their analysis of a line survey of the central parts of the starburst galaxy M82 in the 1.3 mm and 2 mm window, Aladro et al. (2011) found that the physical processes are dominated by PDRs. Arguing that feedback from young OB stars leaves an imprint on molecular composition in the form of an overabundance of CO⁺, HCO, c-C₃H₂, and CH₃CCH, for example, they find M82 to match these criteria. While we can confirm the high c-C₃H₂ emission in our dense PDR region, CH₃CCH is below the 5σ limit there. This is also interesting because their spatial resolution varies between 158 pc and 333 pc, which is 2 to 3 orders of magnitude higher than our averaged spectra, but we observe CH₃CCH emission as quite compact and thus strongly diluted on larger scales. The noise levels are comparable in both studies, ~ 3 – 8 mK for M82, around 8 – 20 mK median noise for the different regions in our Orion data.

5.3. Line ratios on larger scales

Line ratios seem to be more ambiguous on large scales, where both CN(Σ)/HCN(3 – 2) and CN(Σ)/HCO⁺(3 – 2) do not clearly highlight regions with enhanced UV irradiation. We can confirm a correlation between HCN(3 – 2)/HNC(3 – 2) and temperature. On even larger scales, however, as examined by Meier & Turner (2005), among others, for the nuclear region of IC 342 in the 3 mm window (~ 50 pc resolution), the ratio seems to be fairly constant and not related to (kinetic) temperature. Their value of HCN(1 – 0)/HNC(1 – 0) ≈ 1 – 2 is found in our data set for those regions associated with low temperature (see Fig. B.7c). The considered transitions are different to ours, but both species still have comparable upper energies, such that a comparison seems meaningful.

Extragalactic studies like that of Jiménez-Donaire et al. (2017), where the 1 – 0 transitions of HCN, HCO⁺, HNC, and some of their isotopologues are mapped for six nearby galaxies (a few hundred pc to ~ 1 kpc resolution), use spectral stacking to maximise the signal-to-noise ratio for the examined lines. The resulting line ratios of HCN(1 – 0)/HCO⁺(1 – 0) are higher than seen for our regions (HCN(1 – 0)/HCO⁺(1 – 0) = 1.0 – 1.7 vs. HCN(3 – 2)/HCO⁺(3 – 2) = 0.4 – 1.2, see also Fig. 7). Instead, our ratio values are comparable to those found by Harada et al. (2018) in the two nuclei of Merger NGC 3256 (likewise examining the 1 – 0 transitions, ~ 300 pc resolution), although the ratio is critically discussed in this context mainly as a diagnostic for AGN and/or starburst galaxies. Dense gas tracers (1 – 0 transitions) for nine nearby massive spiral galaxies were further examined for the EMPIRE survey (Jiménez-Donaire et al. 2019),

a continuation of these authors' 2017 work. Their Table 4 shows the dense gas line ratios averaged over their galaxy sample, separated into the center (inner 30'', 1–2 kpc resolution) and the disc. Their values of ~ 0.018–0.034 for the HCN(1–0)/CO(1–0) ratio are found in our 1.3 mm data for regions associated with low column density and low temperature, while higher column density regions have a higher value (e.g. HCN(3 – 2)/CO(2 – 1) = 0.18 for the 'high column density' environment). Our HCO⁺/CO values are always higher than theirs (HCO⁺(3 – 2)/CO(2 – 1) ~ 0.050 – 0.156 vs. HCO⁺(1 – 0)/CO(1 – 0) ~ 0.014 – 0.025), the most similar again associated with lower column density regions. Their values for HNC(1 – 0)/CO(1 – 0) (~ 0.010 – 0.014) can also be found in our data, where we find deviations towards higher values to be associated with higher column density regions (e.g. HNC(3 – 2)/CO(2 – 1) ~ 0.04 for the 'high column density' environment).

The correlation of N₂H⁺(3 – 2)/CH₃OH(Σ) with temperature we found on larger scales might be explained both with the temperature sensitivity of N₂H⁺ and the association of CH₃OH with shocks. If temperatures rise, more CO can enter the gas phase and subsequently destroy N₂H⁺, while more CH₃OH evaporates.

6. Summary

We have conducted an imaging line survey of OMC-1 to OMC-3 from 200.2 to 281.8 GHz and examined the emission of distinct regions. These were selected to represent regimes of low or high column density and differing temperature, but also to cover the influence of UV irradiation. By contrasting their emission with each other, we aim to provide templates for the interpretation of other more distant, spatially unresolved sources. Comparing spectra from these unresolved sources with our different templates might reveal similarities that can help to further characterise the distant object. The transitions of the 29 species (55 isotopologues) listed in Table A.1 were considered for the analysis. The integrated intensity of a given species is considered here to be the sum over all of their respective transitions. From our analysis we would like to highlight the following results:

1. Line emission from an Orion KL-like source can contribute significantly to spectra averaged over larger regions, both in terms of averaged total intensity and chemical diversity. In terms of line luminosities, KL and Orion South contribute around 25% of all emission in the 1.3 mm window in the area of OMC-1 to OMC-3.
2. Regions like OMC-2/3, with pre-stellar Class 0 and Class I objects and enhanced column density but low temperature, have a much lower total intensity. Their signatures (e.g. high N₂H⁺ emission coincident with a low HCN(3–2)/HNC(3–2) ratio) would be difficult to pick up in a non-resolved source.
3. While the contribution of CO to the share of the total intensity can vary more strongly in the examined 1.3 mm window, HCO⁺(3 – 2) contributes ~ 3% – 6% in all cases (average ≈ 4%). This seems to hold true even in the case of the emission around KL and Orion South.
4. The emissions of the high-density tracers HCN, HCO⁺, H₂CO, HNC, CS, but also CN are strongly correlated with each other, but not with N₂H⁺. Of all the examined species, N₂H⁺ shows the strongest correlation with column density. If N₂H⁺ observations are not available, HNC seems to trace the column density most reliably.
5. Around 50% of the line luminosity of HCO⁺ and HNC in the 1.3 mm window comes from lower column density material, for CS and HCN ~ 35%.

6. The ratios $\text{HCN}(3-2)/\text{HNC}(3-2)$ and $\text{N}_2\text{H}^+(3-2)/\text{CH}_3\text{OH}(\Sigma)$ may be related to temperature.
7. Identifying UV illuminated material on large scales seems to be challenging, as both $\text{CN}(\Sigma)/\text{HCN}(3-2)$ and $\text{CN}(\Sigma)/\text{HCO}^+(3-2)$ show ambiguous results.

Acknowledgements. We thank the anonymous referee for their careful reading of the manuscript and helpful comments that improved the article. DC acknowledges support by the Deutsche Forschungsgemeinschaft, DFG through project number SFB956C.

References

- Aladro, R., Martín, S., Martín-Pintado, J., et al. 2011, *A&A*, 535, A84
 Bachiller, R. & Pérez Gutiérrez, M. 1997, *ApJ*, 487, L93
 Berné, O., Marcelino, N., & Cernicharo, J. 2014, *ApJ*, 795, 13
 Blake, G. A., Sutton, E. C., Masson, C. R., & Phillips, T. G. 1987, *ApJ*, 315, 621
 Bron, E., Daudon, C., Pety, J., et al. 2018, *A&A*, 610, A12
 Chini, R., Reipurth, B., Ward-Thompson, D., et al. 1997, *ApJ*, 474, L135
 Endres, C. P., Schlemmer, S., Schilke, P., Stutzki, J., & Müller, H. S. P. 2016, *Journal of Molecular Spectroscopy*, 327, 95
 Esplugues, G. B., Tercero, B., Cernicharo, J., et al. 2013, *A&A*, 556, A143
 Foster, J. B., Jackson, J. M., Barnes, P. J., et al. 2011, *ApJS*, 197, 25
 Foster, J. B., Rathborne, J. M., Sanhueza, P., et al. 2013, *PASA*, 30, e038
 Friesen, R. K., Pineda, J. E., co-PIs, et al. 2017, *ApJ*, 843, 63
 Galli, D., Walmsley, M., & Gonçalves, J. 2002, *A&A*, 394, 275
 Goldsmith, P. F. 2001, *ApJ*, 557, 736
 Goldsmith, P. F. & Kauffmann, J. 2017, *ApJ*, 841, 25
 Graninger, D. M., Herbst, E., Öberg, K. I., & Vasyunin, A. I. 2014, *ApJ*, 787, 74
 Gratier, P., Bron, E., Gerin, M., et al. 2017, *A&A*, 599, A100
 Greaves, J. S. & White, G. J. 1992, *MNRAS*, 259, 457
 Güsten, R., Nyman, L. Å., Schilke, P., et al. 2006, *A&A*, 454, L13
 Guzmán, A. E., Sanhueza, P., Contreras, Y., et al. 2015, *ApJ*, 815, 130
 Harada, N., Sakamoto, K., Martín, S., et al. 2018, *ApJ*, 855, 49
 Jackson, J. M., Rathborne, J. M., Foster, J. B., et al. 2013, *PASA*, 30, e057
 Jiménez-Donaire, M. J., Bigiel, F., Leroy, A. K., et al. 2017, *MNRAS*, 466, 49
 Jiménez-Donaire, M. J., Bigiel, F., Leroy, A. K., et al. 2019, *ApJ*, 880, 127
 Johnstone, D. & Bally, J. 1999, *ApJ*, 510, L49
 Johnstone, D., Boonman, A. M. S., & van Dishoeck, E. F. 2003, *A&A*, 412, 157
 Jones, E., Oliphant, T., Peterson, P., et al. 2001-2019, *SciPy: Open source scientific tools for Python*
 Kauffmann, J., Goldsmith, P. F., Melnick, G., et al. 2017, *A&A*, 605, L5
 Kounkel, M. 2017, PhD thesis, University of Michigan
 Lis, D. C., Serabyn, E., Keene, J., et al. 1998, *ApJ*, 509, 299
 Liszt, H. S. & Pety, J. 2016, *ApJ*, 823, 124
 Maret, S., Hily-Blant, P., Pety, J., Bardeau, S., & Reynier, E. 2011, *A&A*, 526, A47
 Masson, C. R., Berge, G. L., Claussen, M. J., et al. 1984, *ApJ*, 283, L37
 Meier, D. S. & Turner, J. L. 2005, *ApJ*, 618, 259
 Menten, K. M., Reid, M. J., Forbrich, J., & Brunthaler, A. 2007, *A&A*, 474, 515
 Nagy, Z., van der Tak, F. F. S., Fuller, G. A., & Plume, R. 2015, *A&A*, 577, A127
 O'Dell, C. R., Muench, A., Smith, N., & Zapata, L. 2008, *Star Formation in the Orion Nebula II: Gas, Dust, Proplyds and Outflows*, ed. B. Reipurth, 544
 Pabst, C., Higgins, R., Goicoechea, J. R., et al. 2019, *Nature*, 565, 618
 Peterson, D. E. & Megeath, S. T. 2008, *The Orion Molecular Cloud 2/3 and NGC 1977 Regions*, ed. B. Reipurth, 590
 Peterson, D. E., Megeath, S. T., Luhman, K. L., et al. 2008, *ApJ*, 685, 313
 Pety, J., Guzmán, V. V., Orkisz, J. H., et al. 2017, *A&A*, 599, A98
 Pickett, H. M., Poynter, R. L., Cohen, E. A., et al. 1998, *J. Quant. Spec. Radiat. Transf.*, 60, 883
 Sakai, N., Ceccarelli, C., Bottinelli, S., Sakai, T., & Yamamoto, S. 2012, *ApJ*, 754, 70
 Schilke, P., Groesbeck, T. D., Blake, G. A., Phillips, & T. G. 1997, *ApJS*, 108, 301
 Shirley, Y. L. 2015, *PASP*, 127, 299
 Sutton, E. C., Blake, G. A., Masson, C. R., & Phillips, T. G. 1985, *ApJS*, 58, 341
 Tang, X. D., Henkel, C., Menten, K. M., et al. 2018, *A&A*, 609, A16
 Tercero, B., Cernicharo, J., Pardo, J. R., & Goicoechea, J. R. 2010, *A&A*, 517, A96
 Tercero, B., Vincent, L., Cernicharo, J., Viti, S., & Marcelino, N. 2011, *A&A*, 528, A26
 Turner, B. E. & Thaddeus, P. 1977, *ApJ*, 211, 755
 Ungerechts, H., Bergin, E. A., Goldsmith, P. F., et al. 1997, *ApJ*, 482, 245
 Wakelam, V., Caselli, P., Ceccarelli, C., Herbst, E., & Castets, A. 2004, *A&A*, 422, 159
 Watanabe, Y., Nishimura, Y., Harada, N., et al. 2017, *ApJ*, 845, 116
 Wiseman, J. J. & Ho, P. T. P. 1998, *ApJ*, 502, 676
 Wyrowski, F., Schilke, P., Hofner, P., & Walmsley, C. M. 1997, *ApJ*, 487, L171
 Yu, K. C., Bally, J., & Devine, D. 1997, *ApJ*, 485, L45

Appendix A: Tables

Species	Isotopologue	Frequency [MHz]	Transition	Energy [K]	G _{up}	A _{ij} [s ⁻¹]	Comment		
c-C ₃ H ₂	c-C ₃ H ₂	204788.926	4 _{2,2,0} – 3 _{3,1,0}	28.8	9	1.37e-04	ignored, S/N not good		
		216278.756	3 _{3,0,0} – 2 _{2,1,0}	19.5	21	2.81e-04			
		217822.148	6 _{1,6,0} – 5 _{0,5,0}	38.6	39	5.93e-04			
		217822.148	6 _{0,6,0} – 5 _{1,5,0}	38.6	13	5.93e-04			
		217940.046	5 _{1,4,0} – 4 _{2,3,0}	35.4	33	4.43e-04			
		218160.442	5 _{2,4,0} – 4 _{1,3,0}	35.4	11	4.44e-04			
		227169.127	4 _{3,2,0} – 3 _{2,1,0}	29.1	27	3.42e-04			
		249054.368	5 _{2,3,0} – 4 _{3,2,0}	41.0	33	4.57e-04			
		251314.337	7 _{0,7,0} – 6 _{1,6,0}	50.7	45	9.35e-04			
		251314.343	7 _{1,7,0} – 6 _{0,6,0}	50.7	15	9.35e-04			
		251508.691	6 _{1,5,0} – 5 _{2,4,0}	47.5	13	7.42e-04			
		251527.302	6 _{2,5,0} – 5 _{1,4,0}	47.5	39	7.42e-04			
		254987.640	5 _{3,3,0} – 4 _{2,2,0}	41.1	11	5.17e-04		ignored, S/N not good	
		260479.746	5 _{3,2,0} – 4 _{4,1,0}	44.7	33	1.77e-04		ignored, blended with SiO	
		265759.438	4 _{4,1,0} – 3 _{3,0,0}	32.2	27	7.99e-04			
		CCH	CCH	261978.120	3 _{4,3} – 2 _{3,3}	25.1		7	1.96e-06
262004.260	3 _{4,4} – 2 _{3,3}			25.1	9	5.32e-05			
262006.482	3 _{4,3} – 2 _{3,2}			25.1	7	5.12e-05			
262064.986	3 _{3,3} – 2 _{2,2}			25.2	7	4.89e-05			
262067.469	3 _{3,2} – 2 _{2,1}			25.2	5	4.47e-05			
262078.935	3 _{3,2} – 2 _{2,2}			25.2	5	6.02e-06			
262208.614	3 _{3,3} – 2 _{3,3}			25.2	7	3.96e-06			
262250.929	3 _{3,2} – 2 _{3,2}			25.2	5	2.27e-06			
CCD	CCD			216372.830	3 _{4,5} – 2 _{3,4}	20.8	10	3e-05	
				216373.320	3 _{4,3} – 2 _{3,2}	20.8	6	2.67e-05	
				216373.320	3 _{4,4} – 2 _{3,3}	20.8	8	2.76e-05	
				216428.320	3 _{3,4} – 2 _{2,3}	20.8	8	2.78e-05	
				216428.320	3 _{3,3} – 2 _{2,2}	20.8	6	2.34e-05	
				216428.760	3 _{3,2} – 2 _{2,1}	20.8	4	2.1e-05	
CF ⁺	CF ⁺	205170.520	2 ₀ – 1 ₀	14.8	5	4.62e-05	may be blended with CH ₃ CHO		
CH ₃ CCH	CH ₃ CCH	205018.080	12 ₄ – 11 ₄	179.2	25	2.41e-05	blended with CH ₃ OCH ₃		
		205045.401	12 ₃ – 11 ₃	128.8	50	2.54e-05			
		205065.015	12 ₂ – 11 ₂	92.8	25	2.63e-05			
		205076.775	12 ₁ – 11 ₁	71.2	25	2.69e-05			
		205080.660	12 ₀ – 11 ₀	64.0	25	2.71e-05			
		222099.151	13 ₄ – 12 ₄	189.8	27	3.13e-05			
		222128.808	13 ₃ – 12 ₃	139.4	54	3.27e-05			
		222150.008	13 ₂ – 12 ₂	103.4	27	3.37e-05			
		222162.729	13 ₁ – 12 ₁	81.8	27	3.44e-05			
		222166.970	13 ₀ – 12 ₀	74.6	27	3.46e-05			
		239211.216	14 ₃ – 13 ₃	150.9	58	4.13e-05			
		239234.011	14 ₂ – 13 ₂	114.9	29	4.24e-05			
		239247.727	14 ₁ – 13 ₁	93.3	29	4.31e-05			
		239252.297	14 ₀ – 13 ₀	86.1	29	4.33e-05			
		256292.638	15 ₃ – 14 ₃	163.2	62	5.12e-05			
		256317.078	15 ₂ – 14 ₂	127.2	31	5.24e-05			
		256331.746	11 ₃ – 10 ₃	105.6	31	5.31e-05			
256336.636	15 ₀ – 14 ₀	98.4	31	5.34e-05					
273373.006	16 ₃ – 15 ₃	176.3	66	6.26e-05					
273399.067	16 ₂ – 15 ₂	140.3	33	6.39e-05					
273414.707	16 ₁ – 15 ₁	118.7	33	6.46e-05					
273419.921	16 ₀ – 15 ₀	111.5	33	6.49e-05					
CH ₃ CN	CH ₃ CN	202215.371	11 ₆ – 10 ₆	315.3	92	4.97e-04			
		202258.154	11 ₅ – 10 ₅	236.8	46	5.62e-04			
		202293.183	11 ₄ – 10 ₄	172.6	46	6.15e-04			
		202320.443	11 ₃ – 10 ₃	122.6	92	6.56e-04			
		202339.921	11 ₂ – 10 ₂	86.8	46	6.86e-04			
		202351.612	11 ₁ – 10 ₁	65.4	46	7.03e-04			
		202355.509	11 ₀ – 10 ₀	58.3	46	7.09e-04			
		220594.423	12 ₆ – 11 ₆	325.9	100	6.92e-04			
		220641.084	12 ₅ – 11 ₅	247.4	50	7.63e-04			
		220679.287	12 ₄ – 11 ₄	183.1	50	8.21e-04			
		220709.016	12 ₃ – 11 ₃	133.2	100	8.66e-04			
		220730.261	12 ₂ – 11 ₂	97.4	50	8.98e-04			
		220743.011	12 ₁ – 11 ₁	76.0	50	9.18e-04			
220747.261	12 ₀ – 11 ₀	68.9	50	9.24e-04					

Continued on next page

(Continuation)							
Species	Isotopologue	Frequency	Transition	Energy	G_{up}	A_{ij}	Comment
		238972.389	13 ₆ – 12 ₆	337.4	108	9.26e-04	
		239022.924	13 ₅ – 12 ₅	258.9	54	1e-03	
		239064.299	13 ₄ – 12 ₄	194.6	54	1.07e-03	
		239096.497	13 ₃ – 12 ₃	144.6	108	1.12e-03	
		239119.504	13 ₂ – 12 ₂	108.9	54	1.15e-03	
		239133.313	13 ₁ – 12 ₁	87.5	54	1.17e-03	
		239137.916	13 ₀ – 12 ₀	80.3	54	1.18e-03	
		257349.179	14 ₆ – 13 ₆	349.7	116	1.2e-03	
		257403.584	14 ₅ – 13 ₅	271.2	58	1.29e-03	blended with CH ₃ OH
		257448.128	14 ₄ – 13 ₄	207.0	58	1.35e-03	
		257482.791	14 ₃ – 13 ₃	157.0	116	1.41e-03	
		257507.561	14 ₂ – 13 ₂	121.3	58	1.45e-03	
		257522.427	14 ₁ – 13 ₁	99.8	58	1.47e-03	
		257527.383	14 ₀ – 13 ₀	92.7	58	1.48e-03	
		275724.702	15 ₆ – 14 ₆	363.0	124	1.53e-03	
		275782.974	15 ₅ – 14 ₅	284.5	62	1.62e-03	
		275830.683	15 ₄ – 14 ₄	220.2	62	1.69e-03	
		275867.810	15 ₃ – 14 ₃	170.2	124	1.75e-03	
		275894.340	15 ₂ – 14 ₂	134.5	62	1.79e-03	
		275910.263	15 ₁ – 14 ₁	113.1	62	1.81e-03	
		275915.571	15 ₀ – 14 ₀	105.9	62	1.82e-03	
CH ₃ OH	CH ₃ OH	201071.847	8 _{4,5,0} – 9 _{3,6,0}	163.9	68	9.12e-06	
		201088.939	8 _{4,4,0} – 9 _{3,7,0}	163.9	68	9.12e-06	
		200820.674	15 _{3,12,2} – 14 _{4,11,2}	341.2	124	1.27e-05	
		201445.493	5 _{2,3,0} – 6 _{1,6,0}	72.5	44	1.3e-05	
		201996.513	18 _{1,17,1} – 18 _{0,18,1}	417.9	148	2.92e-05	
		205791.270	1 _{1,1,0} – 2 _{0,2,0}	16.8	12	3.36e-05	
		206001.302	12 _{5,7,1} – 13 _{4,9,1}	317.1	100	1.04e-05	
		209518.804	19 _{1,18,1} – 19 _{0,19,1}	462.0	156	3.13e-05	ignored, blended with CH ₃ OCH ₃
		213377.528	13 _{6,8,1} – 14 _{5,9,1}	389.9	108	1.07e-05	
		213427.061	1 _{1,0,1} – 0 _{0,0,1}	23.4	12	3.37e-05	
		215302.206	6 _{1,6,3} – 7 _{2,6,3}	373.8	52	4.18e-05	
		216945.521	5 _{1,4,1} – 4 _{2,3,1}	55.9	44	1.21e-05	
		217299.205	6 _{1,5,3} – 7 _{2,5,3}	373.9	52	4.28e-05	
		218440.063	4 _{2,3,1} – 3 _{1,2,1}	45.5	36	4.69e-05	
		220078.561	8 _{0,8,1} – 7 _{1,6,1}	96.6	68	2.52e-05	
		220401.317	10 _{5,6,2} – 11 _{4,8,2}	251.6	84	1.12e-05	ignored, blended with ¹³ CO
		227814.528	16 _{1,16,0} – 15 _{2,13,0}	327.2	132	2.18e-05	
		229589.056	15 _{4,11,1} – 16 _{3,14,1}	374.4	124	2.08e-05	
		229758.756	8 _{1,8,2} – 7 _{0,7,1}	89.1	68	4.19e-05	
		230027.047	3 _{2,1,2} – 4 _{1,4,2}	39.8	28	1.49e-05	
		231281.110	10 _{2,9,0} – 9 _{3,6,0}	165.3	84	1.83e-05	
		232418.521	10 _{2,8,0} – 9 _{3,7,0}	165.4	84	1.87e-05	
		232783.446	18 _{3,16,0} – 17 _{4,13,0}	446.5	148	2.17e-05	
		232945.797	10 _{3,7,2} – 11 _{2,9,2}	190.4	84	2.13e-05	
		233795.666	18 _{3,15,0} – 17 _{4,14,0}	446.6	148	2.2e-05	
		234683.370	4 _{2,3,0} – 5 _{1,4,0}	60.9	36	1.87e-05	
		234698.519	5 _{4,2,2} – 6 _{3,3,2}	122.7	44	6.34e-06	
		236936.089	14 _{1,13,0} – 13 _{2,12,0}	260.2	116	3.11e-05	
		239746.219	5 _{1,5,0} – 4 _{1,4,0}	49.1	44	5.66e-05	
		240241.490	5 _{3,3,1} – 6 _{2,5,1}	82.5	44	1.44e-05	
		240960.557	5 _{1,5,3} – 4 _{1,4,3}	360.0	44	5.76e-05	
		241159.199	5 _{4,2,4} – 4 _{4,1,4}	398.1	44	2.15e-05	
		241166.580	5 _{3,2,4} – 4 _{3,1,4}	452.1	44	3.86e-05	
		241179.886	5 _{3,3,5} – 4 _{3,2,5}	357.4	44	3.83e-05	
		241184.189	5 _{4,1,5} – 4 _{4,0,5}	440.1	44	2.16e-05	
		241187.428	5 _{2,4,5} – 4 _{2,3,5}	399.3	44	5.07e-05	
		241192.856	5 _{2,4,3} – 4 _{2,3,3}	333.4	44	5.03e-05	
		241196.430	5 _{2,3,3} – 4 _{2,2,3}	333.4	44	5.03e-05	
		241198.285	5 _{3,3,3} – 4 _{3,2,3}	430.8	44	3.83e-05	
		241198.291	5 _{3,2,3} – 4 _{3,1,3}	430.8	44	3.83e-05	
		241203.706	5 _{1,5,4} – 4 _{1,4,4}	326.2	44	5.75e-05	
		241206.035	5 _{0,5,4} – 4 _{0,4,4}	335.3	44	6e-05	
		241210.764	5 _{2,3,4} – 4 _{2,2,4}	434.6	44	5.04e-05	
		241238.144	5 _{1,4,5} – 4 _{1,3,5}	448.1	44	5.75e-05	
		241267.862	5 _{0,5,3} – 4 _{0,4,3}	458.4	44	6e-05	
		241441.270	5 _{1,4,3} – 4 _{1,3,3}	360.0	44	5.79e-05	

Continued on next page

(Continuation) Species	Isotopologue	Frequency	Transition	Energy	G _{up}	A _{ij}	Comment
		241700.159	5 _{0,5,1} – 4 _{0,4,1}	47.9	44	6.04e-05	
		241767.234	5 _{1,5,2} – 4 _{1,4,2}	40.4	44	5.81e-05	
		241791.352	5 _{0,5,0} – 4 _{0,4,0}	34.8	44	6.05e-05	
		241806.524	5 _{4,2,0} – 4 _{4,1,0}	115.2	44	2.18e-05	
		241806.525	5 _{4,1,0} – 4 _{4,0,0}	115.2	44	2.18e-05	
		241813.255	5 _{4,2,2} – 4 _{4,1,2}	122.7	44	2.18e-05	
		241829.629	5 _{4,1,1} – 4 _{4,0,1}	130.8	44	2.19e-05	
		241832.718	5 _{3,3,0} – 4 _{3,2,0}	84.6	44	3.87e-05	
		241833.106	5 _{3,2,0} – 4 _{3,1,0}	84.6	44	3.87e-05	
		241842.284	5 _{2,4,0} – 4 _{2,3,0}	72.5	44	5.11e-05	
		241843.604	5 _{3,3,1} – 4 _{3,2,1}	82.5	44	3.88e-05	
		241852.299	5 _{3,2,2} – 4 _{3,1,2}	97.5	44	3.89e-05	
		241879.025	5 _{1,4,1} – 4 _{1,3,1}	55.9	44	5.96e-05	
		241887.674	5 _{2,3,0} – 4 _{2,2,0}	72.5	44	5.12e-05	
		241904.147	5 _{2,3,2} – 4 _{2,2,2}	60.7	44	5.09e-05	
		241904.643	5 _{2,4,1} – 4 _{2,3,1}	57.1	44	5.03e-05	
		242446.084	14 _{1,14,2} – 13 _{2,11,2}	248.9	116	2.29e-05	
		243915.788	5 _{1,4,0} – 4 _{1,3,0}	49.7	44	5.97e-05	
		244337.983	9 _{1,9,4} – 8 _{0,8,4}	395.6	76	4.06e-05	ignored, S/N not good
		246873.301	19 _{3,16,0} – 19 _{2,17,0}	490.7	156	8.27e-05	
		247161.950	16 _{2,15,1} – 15 _{3,13,1}	338.1	132	2.57e-05	
		247228.587	4 _{2,2,0} – 5 _{1,5,0}	60.9	36	2.12e-05	
		247610.918	18 _{3,15,0} – 18 _{2,16,0}	446.6	148	8.29e-05	
		248282.424	17 _{3,14,0} – 17 _{2,15,0}	404.8	140	8.3e-05	
		248885.468	16 _{3,13,0} – 16 _{2,14,0}	365.4	132	8.32e-05	
		249192.836	16 _{3,13,2} – 15 _{4,12,2}	378.3	132	2.54e-05	
		249419.924	15 _{3,12,0} – 15 _{2,13,0}	328.3	124	8.32e-05	
		249443.301	7 _{4,4,0} – 8 _{3,5,0}	145.3	60	1.48e-05	
		249451.842	7 _{4,3,0} – 8 _{3,6,0}	145.3	60	1.48e-05	
		249887.467	14 _{3,11,0} – 14 _{2,12,0}	293.5	116	8.32e-05	
		250291.181	13 _{3,10,0} – 13 _{2,11,0}	261.0	108	8.3e-05	
		250506.853	11 _{0,11,0} – 10 _{1,10,0}	153.1	92	8.46e-05	
		250635.200	12 _{3,9,0} – 12 _{2,10,0}	230.8	100	8.28e-05	
		250924.398	11 _{3,8,0} – 11 _{2,9,0}	203.0	92	8.24e-05	
		251164.108	10 _{3,7,0} – 10 _{2,8,0}	177.5	84	8.18e-05	
		251359.888	9 _{3,6,0} – 9 _{2,7,0}	154.2	76	8.09e-05	
		251517.309	8 _{3,5,0} – 8 _{2,6,0}	133.4	68	7.96e-05	
		251641.787	7 _{3,4,0} – 7 _{2,5,0}	114.8	60	7.76e-05	
		251738.437	6 _{3,3,0} – 6 _{2,4,0}	98.5	52	7.46e-05	
		251811.956	5 _{3,2,0} – 5 _{2,3,0}	84.6	44	6.97e-05	
		251866.524	4 _{3,1,0} – 4 _{2,2,0}	73.0	36	6.1e-05	
		251890.886	5 _{3,3,0} – 5 _{2,4,0}	84.6	44	6.97e-05	
		251895.728	6 _{3,4,0} – 6 _{2,5,0}	98.5	52	7.47e-05	
		251900.452	4 _{3,2,0} – 4 _{2,3,0}	73.0	36	6.1e-05	
		251905.729	3 _{3,0,0} – 3 _{2,1,0}	63.7	28	4.36e-05	
		251917.065	3 _{3,1,0} – 3 _{2,2,0}	63.7	28	4.36e-05	
		251923.701	7 _{3,5,0} – 7 _{2,6,0}	114.8	60	7.78e-05	
		251984.837	8 _{3,6,0} – 8 _{2,7,0}	133.4	68	7.98e-05	
		252090.409	9 _{3,7,0} – 9 _{2,8,0}	154.2	76	8.13e-05	
		252252.849	10 _{3,8,0} – 10 _{2,9,0}	177.5	84	8.25e-05	
		252485.675	11 _{3,9,0} – 11 _{2,10,0}	203.0	92	8.34e-05	
		252803.388	12 _{3,10,0} – 12 _{2,11,0}	230.8	100	8.42e-05	
		253221.376	13 _{3,11,0} – 13 _{2,12,0}	261.0	108	8.49e-05	
		253755.809	14 _{3,12,0} – 14 _{2,13,0}	293.5	116	8.56e-05	
		254015.377	2 _{0,2,1} – 1 _{1,1,2}	20.1	20	1.9e-05	
		254419.419	11 _{5,6,1} – 12 _{4,8,1}	289.2	92	1.79e-05	
		254423.520	15 _{3,13,0} – 15 _{2,14,0}	328.3	124	8.63e-05	
		255241.888	16 _{3,14,0} – 16 _{2,15,0}	365.4	132	8.71e-05	
		256228.714	17 _{3,15,0} – 17 _{2,16,0}	404.8	140	8.8e-05	
		257402.086	18 _{3,16,0} – 18 _{2,17,0}	446.5	148	8.9e-05	ignored, blended with CH ₃ CN
		258780.248	19 _{3,17,0} – 19 _{2,18,0}	490.6	156	9.01e-05	
		261704.409	12 _{6,7,1} – 13 _{5,8,1}	359.8	100	1.78e-05	
		261805.675	2 _{1,1,1} – 1 _{0,1,1}	28.0	20	5.57e-05	
		263793.875	5 _{1,5,3} – 6 _{2,5,3}	360.0	44	8.22e-05	ignored, blended with HCCCN
		265224.426	5 _{1,4,3} – 6 _{2,4,3}	360.0	44	8.33e-05	
		265289.562	6 _{1,5,1} – 5 _{2,4,1}	69.8	52	2.58e-05	
		266838.148	5 _{2,4,1} – 4 _{1,3,1}	57.1	44	7.74e-05	

Continued on next page

(Continuation)							
Species	Isotopologue	Frequency	Transition	Energy	G_{up}	A_{ij}	Comment
		267403.471	$9_{0,9,1} - 8_{1,7,1}$	117.5	76	4.67e-05	
		267406.071	$17_{1,17,0} - 16_{2,14,0}$	366.3	140	3.51e-05	
		268743.954	$9_{5,5,2} - 10_{4,7,2}$	228.4	76	1.76e-05	
		278304.512	$9_{1,9,2} - 8_{0,8,1}$	110.0	76	7.69e-05	
		278342.261	$2_{2,0,2} - 3_{1,3,2}$	32.9	20	1.65e-05	
		278599.037	$14_{4,10,1} - 15_{3,13,1}$	339.6	116	3.6e-05	ignored, S/N not good
		279351.887	$11_{2,10,0} - 10_{3,7,0}$	190.9	92	3.45e-05	
		280679.621	$19_{3,17,0} - 18_{4,14,0}$	490.6	156	3.87e-05	ignored, S/N not good
		281000.109	$11_{2,9,0} - 10_{3,8,0}$	190.9	92	3.53e-05	
CN	CN	226287.418	$2_{0,2,1} - 1_{0,2,1}$	16.3	2	1.03e-05	
		226298.943	$2_{0,2,1} - 1_{0,2,2}$	16.3	2	8.23e-06	
		226303.037	$2_{0,2,2} - 1_{0,2,1}$	16.3	4	4.17e-06	
		226314.540	$2_{0,2,2} - 1_{0,2,2}$	16.3	4	9.91e-06	
		226332.499	$2_{0,2,2} - 1_{0,2,3}$	16.3	4	4.56e-06	
		226341.930	$2_{0,2,3} - 1_{0,2,2}$	16.3	6	3.16e-06	
		226359.871	$2_{0,2,3} - 1_{0,2,3}$	16.3	6	1.61e-05	
		226616.571	$2_{0,2,1} - 1_{0,1,2}$	16.3	2	1.07e-05	
		226632.190	$2_{0,2,2} - 1_{0,1,2}$	16.3	4	4.26e-05	
		226659.558	$2_{0,2,3} - 1_{0,1,2}$	16.3	6	9.47e-05	ignored, frequency gap
		226663.693	$2_{0,2,1} - 1_{0,1,1}$	16.3	2	8.47e-05	
		226679.311	$2_{0,2,2} - 1_{0,1,1}$	16.3	4	5.27e-05	
		226874.191	$2_{0,3,3} - 1_{0,2,2}$	16.3	6	9.62e-05	partially blanked (*)
		226874.781	$2_{0,3,4} - 1_{0,2,3}$	16.3	8	1.14e-04	partially blanked (*)
		226875.896	$2_{0,3,2} - 1_{0,2,1}$	16.3	4	8.59e-05	partially blanked (*)
		226887.420	$2_{0,3,2} - 1_{0,2,2}$	16.3	4	2.73e-05	
		226892.128	$2_{0,3,3} - 1_{0,2,3}$	16.3	6	1.81e-05	
		226905.357	$2_{0,3,2} - 1_{0,2,3}$	16.3	4	1.13e-06	ignored, S/N not good
	^{13}CN	217467.150	$2_{3,3,4} - 1_{2,2,3}$	15.7	9	1.01e-04	
CO	CO	230538.000	2-1	16.6	5	6.91e-07	
	^{13}CO	220398.684	2-1	15.9	5	6.08e-07	
	C^{18}O	219560.357	2-1	15.8	5	6.01e-07	
	C^{17}O	224714.385	2-1	16.2	5	6.43e-07	
	$^{13}\text{C}^{18}\text{O}$	209419.138	$2_2 - 1_1$	15.1	4	4.36e-07	
		209419.172	$2_3 - 1_2$	15.1	6	5.23e-07	
CS	CS	244935.644	5-4	35.3	11	3e-04	
	^{13}CS	231220.996	5-4	33.3	11	2.52e-04	
		277455.481	6-5	46.6	13	4.42e-04	
	C^{34}S	241016.194	5-4	34.7	11	2.86e-04	
	C^{33}S	242913.610	$5_0 - 4_0$	35.0	44	2.91e-04	
HCCCN	HCCCN	209230.234	23-22	120.5	141	7.24e-04	
		218324.788	24-23	131.0	147	8.23e-04	
		227418.906	25-24	141.9	153	9.31e-04	
		236512.777	26-25	153.2	159	1.05e-03	
		245606.308	27-26	165.0	165	1.17e-03	
		254699.500	28-27	177.3	171	1.31e-03	
		263792.308	29-28	189.9	177	1.46e-03	blended with CH_3OH
		272884.734	30-29	203.0	183	1.61e-03	
HCN	HCN	265886.180	3-2	25.5	21	8.42e-04	
	DCN	217238.400	$3_2 - 2_1$	20.9	5	3.83e-04	
		217238.631	$3_2 - 2_2$	20.9	5	7.08e-05	
		217238.631	$3_3 - 2_3$	20.9	7	5.06e-05	
		217238.631	$3_3 - 2_2$	20.9	7	4.05e-04	
		217238.631	$3_4 - 2_3$	20.9	9	4.55e-04	
	H^{13}CN	259011.821	$3_2 - 2_2$	24.9	5	1.2e-04	
		259011.821	$3_3 - 2_3$	24.9	7	8.58e-05	
		259011.821	$3_2 - 2_1$	24.9	5	6.48e-04	
		259011.821	$3_3 - 2_2$	24.9	7	6.86e-04	
		259011.821	$3_4 - 2_3$	24.9	9	7.72e-04	
	HC^{15}N	258157.100	3-2	24.8	7	7.65e-04	
HCO	HCO	260060.329	$3_{0,3,4,4} - 2_{0,2,3,3}$	25.0	9	1.63e-04	
		260082.192	$3_{0,3,4,3} - 2_{0,2,3,2}$	25.0	7	1.61e-04	
		260133.586	$3_{0,3,3,3} - 2_{0,2,2,2}$	25.0	7	1.45e-04	
		260155.769	$3_{0,3,3,2} - 2_{0,2,2,1}$	25.0	5	1.37e-04	
HCO^+	HCO^+	267557.626	3-2	25.7	7	1.45e-03	blended with SO_2 and OCS
	DCO^+	216112.582	3-2	20.7	7	7.66e-04	
	H^{13}CO^+	260255.339	3-2	25.0	7	1.34e-03	
	HC^{18}O^+	255479.389	3-2	24.5	7	1.27e-03	

Continued on next page

(Continuation)							
Species	Isotopologue	Frequency	Transition	Energy	G _{up}	A _{ij}	Comment
	HC ¹⁷ O ⁺	261164.920	3-2	25.1	42	1.35e-03	
HCS ⁺	HCS ⁺	213360.650	5-4	30.7	11	1.97e-04	
		256027.100	6-5	43.0	13	3.46e-04	
HDO	HDO	225896.720	3 _{1,2} – 2 _{2,1}	167.6	7	1.32e-05	
		241561.550	2 _{1,1} – 2 _{1,2}	95.2	5	1.19e-05	
		266161.070	2 _{2,0} – 3 _{1,3}	157.2	5	1.75e-05	
H ₂ CCO	H ₂ CCO	202014.311	10 _{0,10} – 9 _{0,9}	53.3	21	9.24e-05	ignored, S/N not good
		203940.225	10 _{1,9} – 9 _{1,8}	66.9	63	9.41e-05	
		220177.569	11 _{1,11} – 10 _{1,10}	76.5	69	1.19e-04	
		222197.635	11 _{0,11} – 10 _{0,10}	64.0	23	1.24e-04	
		224327.250	11 _{1,10} – 10 _{1,9}	77.7	69	1.26e-04	
		240185.794	12 _{1,12} – 11 _{1,11}	88.0	75	1.55e-04	
		242375.735	12 _{0,12} – 11 _{0,11}	75.6	25	1.61e-04	ignored, S/N not good
		244712.269	12 _{1,11} – 11 _{11,0}	89.4	75	1.64e-04	
		260191.982	13 _{1,13} – 12 _{1,12}	100.5	81	1.98e-04	
		262548.207	13 _{0,13} – 12 _{0,12}	88.2	27	2.05e-04	ignored, S/N not good
		265095.049	13 _{1,12} – 12 _{1,11}	102.1	81	2.1e-04	
H ₂ CO	H ₂ CO	211211.468	3 _{1,3} – 2 _{1,2}	32.1	21	2.27e-04	
		216568.651	9 _{1,8} – 9 _{1,9}	174.0	57	7.22e-06	
		218222.192	3 _{0,3} – 2 _{0,2}	21.0	7	2.82e-04	
		218475.632	3 _{2,2} – 2 _{2,1}	68.1	7	1.57e-04	
		218760.066	3 _{2,1} – 2 _{2,0}	68.1	7	1.58e-04	
		225697.775	3 _{1,2} – 2 _{1,1}	33.4	21	2.77e-04	
		264270.140	10 _{1,9} – 10 _{1,10}	209.9	63	1.08e-05	
		281526.929	4 _{1,4} – 3 _{1,3}	45.6	27	5.88e-04	
	HDCO	201341.350	3 _{1,2} – 2 _{1,1}	27.3	7	1.96e-04	
		246924.600	4 _{1,4} – 3 _{1,3}	37.6	9	3.96e-04	
		256585.430	4 _{0,4} – 3 _{0,3}	30.8	9	4.74e-04	
		257748.760	4 _{2,3} – 3 _{2,2}	62.8	9	3.6e-04	
		259034.910	4 _{2,2} – 3 _{2,1}	62.9	9	3.66e-04	
		268292.020	4 _{1,3} – 3 _{1,2}	40.2	9	5.08e-04	
	H ₂ ¹³ CO	206131.626	3 _{1,3} – 2 _{1,2}	31.6	21	2.11e-04	
		212811.184	3 _{0,3} – 2 _{0,2}	20.4	7	2.61e-04	
		219908.525	3 _{1,2} – 2 _{1,1}	32.9	21	2.56e-04	
		274762.112	4 _{1,4} – 3 _{1,3}	44.8	27	5.47e-04	
H ₂ CS	H ₂ CS	202923.515	6 _{1,6} – 5 _{1,5}	47.3	39	1.18e-04	
		205987.391	6 _{0,6} – 5 _{0,5}	34.6	13	1.27e-04	
		206053.584	6 _{2,5} – 5 _{2,4}	87.3	13	1.13e-04	
		206158.016	6 _{2,4} – 5 _{2,3}	87.3	13	1.13e-04	ignored, blended with SO
		209200.101	6 _{1,5} – 5 _{1,4}	48.3	39	1.3e-04	
		236726.770	7 _{1,7} – 6 _{1,6}	58.6	45	1.91e-04	
		240266.320	7 _{0,7} – 6 _{0,6}	46.1	15	2.04e-04	
		240381.750	7 _{2,6} – 6 _{2,5}	98.9	15	1.88e-04	
		240548.229	7 _{2,5} – 6 _{2,4}	98.9	15	1.88e-04	
		244047.840	7 _{1,6} – 6 _{1,5}	60.0	45	2.1e-04	
		270520.740	8 _{1,8} – 7 _{1,7}	71.6	51	2.9e-04	
		274520.870	8 _{0,8} – 7 _{0,7}	59.3	17	3.07e-04	
		274702.055	8 _{2,7} – 7 _{2,6}	112.0	17	2.89e-04	
		274952.473	8 _{2,6} – 7 _{2,5}	112.1	17	2.9e-04	
		278886.400	8 _{1,7} – 7 _{1,6}	73.4	51	3.17e-04	
	HDCS	212648.339	7 _{1,7} – 6 _{1,6}	49.8	15	1.39e-04	
		216662.429	7 _{0,7} – 6 _{0,6}	41.6	15	1.5e-04	
	H ₂ C ³⁴ S	202492.418	6 _{0,6} – 5 _{0,5}	34.0	13	1.21e-04	
H ₂ S	H ₂ S	216710.435	2 _{2,0} – 2 _{1,1}	84.0	5	4.83e-05	
HNC	HNC	271981.142	3-2	26.1	7	9.34e-04	
	DNC	228910.489	3-2	22.0	7	5.57e-04	
	HN ¹³ C	261263.310	3-2	25.1	7	6.48e-04	
HNCO	HNCO	218981.009	10 _{1,10} – 9 _{1,9}	101.1	21	1.42e-04	
		219798.274	10 _{0,10} – 9 _{0,9}	58.0	21	1.47e-04	
		220584.751	10 _{1,9} – 9 _{1,8}	101.5	21	1.45e-04	
		240875.727	11 _{1,11} – 10 _{1,10}	112.6	23	1.9e-04	
		241774.032	11 _{0,11} – 10 _{0,10}	69.6	23	1.96e-04	
		242639.704	11 _{1,10} – 10 _{1,9}	113.1	23	1.95e-04	
		262769.477	12 _{1,12} – 11 _{1,11}	125.3	25	2.48e-04	
		263748.625	12 _{0,12} – 11 _{0,11}	82.3	25	2.56e-04	
		264693.655	12 _{1,11} – 11 _{1,10}	125.9	25	2.54e-04	
N ₂ H ⁺	N ₂ H ⁺	279511.701	3-2	26.8	63	1.26e-03	

Continued on next page

(Continuation)								
Species	Isotopologue	Frequency	Transition	Energy	G _{up}	A _{ij}	Comment	
	N ₂ D ⁺	231321.665	3-2	22.2	21	7.14e-04		
NO	NO	250436.848	3 _{1,3,4} - 2 _{-1,2,3}	19.2	8	1.84e-06		
		250440.659	3 _{1,3,3} - 2 _{-1,2,2}	19.2	6	1.55e-06		
		250448.530	3 _{1,3,2} - 2 _{-1,2,1}	19.2	4	1.38e-06		
		250796.436	3 _{-1,3,4} - 2 _{1,2,3}	19.3	8	1.85e-06		
		250815.594	3 _{-1,3,3} - 2 _{1,2,2}	19.3	6	1.55e-06		
		250816.954	3 _{-1,3,2} - 2 _{1,2,1}	19.3	4	1.39e-06		
NS	NS	207436.246	5 _{1,-1,6} - 4 _{1,1,5}	27.6	12	1.51e-04		
		207436.246	5 _{1,-1,5} - 4 _{1,1,4}	27.6	10	1.44e-04		
		207438.692	5 _{1,-1,4} - 4 _{1,1,3}	27.6	8	1.42e-04		
		207834.866	5 _{1,1,6} - 4 _{1,-1,5}	27.7	12	1.52e-04		
		207838.365	5 _{1,1,5} - 4 _{1,-1,4}	27.7	10	1.45e-04		
		207838.365	5 _{1,1,4} - 4 _{1,-1,3}	27.7	8	1.43e-04		
		253570.476	6 _{1,1,7} - 5 _{1,-1,6}	39.8	14	2.83e-04		
		253570.476	6 _{1,1,6} - 5 _{1,-1,5}	39.8	12	2.73e-04		
		253572.148	6 _{1,1,5} - 5 _{1,-1,4}	39.8	10	2.71e-04		
		253968.393	6 _{1,-1,7} - 5 _{1,1,6}	39.9	14	2.84e-04		
		253970.581	6 _{1,-1,6} - 5 _{1,1,5}	39.9	12	2.75e-04		
		253970.581	6 _{1,-1,5} - 5 _{1,1,4}	39.9	10	2.73e-04		
		OCS	OCS	206745.161	17-16	89.3	35	2.55e-05
218903.356	18-17			99.8	37	3.04e-05		
231060.983	19-18			110.9	39	3.58e-05		
243218.040	20-19			122.6	41	4.18e-05		
255374.461	21-20			134.8	43	4.84e-05		
267530.239	22-21			147.7	45	5.57e-05	ignored, blended with HCO ⁺	
279685.318	23-22			161.1	47	6.37e-05		
SiO	SiO	217104.980	5-4	31.3	11	5.21e-04		
		260518.020	6-5	43.8	13	9.15e-04	blended with c-C ₃ H ₂	
	²⁹ SiO	214385.036	5-4	30.9	11	5e-04		
		257254.227	6-5	43.2	13	8.78e-04		
	³⁰ SiO	211852.797	5-4	30.5	11	4.83e-04		
		254215.845	6-5	42.7	13	8.47e-04		
SO	SO	206176.005	5 ₄ - 4 ₃	38.6	9	1.03e-04	blended with H ₂ CS	
		214357.039	8 ₇ - 7 ₇	81.2	15	3.42e-06		
		215220.653	5 ₅ - 4 ₄	44.1	11	1.22e-04		
		219949.442	5 ₆ - 4 ₅	35.0	13	1.36e-04		
		236452.325	2 ₁ - 1 ₂	15.8	3	1.45e-06	ignored, S/N not good	
		246404.687	3 ₂ - 2 ₃	21.1	5	1.03e-06	ignored, S/N not good	
		251825.770	6 ₅ - 5 ₄	50.7	11	1.96e-04		
		254573.500	9 ₈ - 8 ₈	99.7	17	4.32e-06		
		258255.813	6 ₆ - 5 ₅	56.5	13	2.16e-04		
		261843.684	6 ₇ - 5 ₆	47.6	15	2.33e-04		
		³⁴ SO	201846.573	5 ₄ - 4 ₃	38.1	9	9.66e-05	
			211013.673	5 ₅ - 4 ₄	43.5	11	1.15e-04	ignored, frequency gap
			215839.436	5 ₆ - 4 ₅	34.4	13	1.29e-04	
			246663.638	6 ₅ - 5 ₄	49.9	11	1.84e-04	
			253208.020	6 ₆ - 5 ₅	55.7	13	2.04e-04	
256877.456	6 ₇ - 5 ₆	46.7	15	2.2e-04				
SO ⁺	SO ⁺	208590.016	5 _{1,5} - 4 _{-1,4}	26.7	10	4.7e-05	blended with CH ₃ OCH ₃	
		208965.420	5 _{-1,5} - 4 _{1,4}	26.8	10	4.72e-05	blended with C ₂ H ₃ CN	
		254977.935	6 _{-1,6} - 5 _{1,5}	38.9	12	8.77e-05	blended with C ₂ H ₅ CN	
		255353.237	6 _{1,6} - 5 _{-1,5}	39.0	12	8.81e-05		
SO ₂	SO ₂	200809.180	16 _{1,15} - 16 _{0,16}	130.7	33	4.7e-05		
		203391.550	12 _{0,12} - 11 _{1,11}	70.1	25	8.8e-05		
		204246.760	18 _{3,15} - 18 _{2,16}	180.6	37	9.27e-05		
		204384.300	7 _{4,4} - 8 _{3,5}	65.5	15	1.11e-05		
		205300.570	11 _{2,10} - 11 _{1,11}	70.2	23	5.32e-05		
		208700.320	3 _{2,2} - 2 _{1,1}	15.3	7	6.72e-05		
		209936.050	12 _{5,7} - 13 _{4,10}	133.0	25	1.59e-05		
		213068.400	26 _{3,23} - 26 _{2,24}	350.8	53	1.16e-04		
		214689.380	16 _{3,13} - 16 _{2,14}	147.8	33	9.9e-05		
		214728.330	17 _{6,12} - 18 _{5,13}	229.0	35	1.89e-05		
		216643.300	22 _{2,20} - 22 _{1,21}	248.4	45	9.27e-05		
		221965.210	11 _{1,11} - 10 _{0,10}	60.4	23	1.14e-04		
		223883.569	6 _{4,2} - 7 _{3,5}	58.6	13	1.16e-05		
		224264.811	20 _{2,18} - 19 _{3,17}	207.8	41	3.94e-05		
		225153.702	13 _{2,12} - 13 _{1,13}	93.0	27	6.52e-05		

Continued on next page

(Continuation) Species	Isotopologue	Frequency	Transition	Energy	G_{up}	A_{ij}	Comment
		226300.027	14 _{3,11} – 14 _{2,12}	119.0	29	1.07e-04	
		229347.628	11 _{5,7} – 12 _{4,8}	122.0	23	1.91e-05	
		234421.586	16 _{6,10} – 17 _{5,13}	213.3	33	2.35e-05	
		235151.720	4 _{2,2} – 3 _{1,3}	19.0	9	7.69e-05	
		236216.685	16 _{1,15} – 15 _{2,14}	130.7	33	7.5e-05	
		237068.870	12 _{3,9} – 12 _{2,10}	94.0	25	1.14e-04	
		240942.791	18 _{1,17} – 18 _{0,18}	163.1	37	7.02e-05	
		241615.798	5 _{2,4} – 4 _{1,3}	23.6	11	8.45e-05	
		243087.647	5 _{4,2} – 6 _{3,3}	53.1	11	1.03e-05	
		244254.218	14 _{0,14} – 13 _{1,13}	93.9	29	1.64e-04	
		245563.423	10 _{3,7} – 10 _{2,8}	72.7	21	1.19e-04	
		248057.401	15 _{2,14} – 15 _{1,15}	119.3	31	8.06e-05	
		248830.824	10 _{5,5} – 11 _{4,8}	111.9	21	2.19e-05	
		251199.675	13 _{1,13} – 12 _{0,12}	82.2	27	1.76e-04	
		251210.586	8 _{3,5} – 8 _{2,6}	55.2	17	1.2e-04	
		253956.567	15 _{6,10} – 16 _{5,11}	198.6	31	2.82e-05	ignored, possibly artifact
		254280.536	6 _{3,3} – 6 _{2,4}	41.4	13	1.14e-04	
		254283.319	24 _{2,22} – 24 _{1,23}	292.7	49	1.33e-04	
		255553.303	4 _{3,1} – 4 _{2,2}	31.3	9	9.28e-05	
		255958.044	3 _{3,1} – 3 _{2,2}	27.6	7	6.63e-05	
		256246.946	5 _{3,3} – 5 _{2,4}	35.9	11	1.07e-04	
		257099.966	7 _{3,5} – 7 _{2,6}	47.8	15	1.22e-04	
		258942.199	9 _{3,7} – 9 _{2,8}	63.5	19	1.32e-04	
		262256.905	11 _{3,9} – 11 _{2,10}	82.8	23	1.41e-04	
		267537.450	13 _{3,11} – 13 _{2,12}	105.8	27	1.51e-04	ignored, blended with HCO ⁺
		268168.334	9 _{5,5} – 10 _{4,6}	102.7	19	2.39e-05	
		271529.015	7 _{2,6} – 6 _{1,5}	35.5	15	1.11e-04	
		273462.668	14 _{6,8} – 15 _{5,11}	184.8	29	3.3e-05	
		273752.961	17 _{2,16} – 17 _{1,17}	149.2	35	9.97e-05	
		275240.182	15 _{3,13} – 15 _{2,14}	132.5	31	1.64e-04	
		280807.280	26 _{4,22} – 26 _{3,23}	364.3	53	2.33e-04	

Table A.1: All considered transitions for our fitting procedure. The comments are based on the spectrum of the high column density region. Notes concerning overlap between lines, especially with complex organic molecules, are thus likely not relevant on larger scales or for low column density/low temperature regions. Lines ignored due to e.g. locally too poor S/N are marked as such. In case of a strong overlap and one line being significantly stronger than the other (e.g. overlap with HCO⁺), the area is contributed to the stronger line only. (*) Three CN transitions are strongly blended and part of this line falls into a gap in the frequency coverage. A Gauss fit is still possible, and we made sure that the fitted line has no peak intensity larger than the visible part of the line.

Table A.2: Uncertainties for the averaged total intensities $\Delta \int T_{\text{mb}} d\nu$ [K km s⁻¹] from Table 4.

species	all averaged	high column density	high column density without KL and Orion South	high column density, low temperature	high column density, high temperature, without KL and Orion South	low column density	low temperature	low column density, low temperature	low column density, high temperature	high temperature without KL and Orion South	H II	radical region	dense PDR
CO	0.01	0.03	0.12	0.06	0.03	0.60	0.01	0.01	7.13	0.64	0.01	0.01	0.03
¹³ CO	0.01	0.01	<0.01	0.01	0.01	<0.01	0.02	0.11	<0.01	0.02	0.01	0.01	<0.01
C ¹⁸ O	0.08	<0.01	0.01	0.03	0.04	0.02	0.28	0.02	0.07	0.01	0.05	0.03	0.25
C ¹⁷ O	0.14	0.11	0.15	0.01	0.35	0.15	0.03	0.02	0.02	0.03	0.76	0.35	0.29
¹³ C ¹⁸ O	-	0.02	0.01	0.02	0.01	-	0.02	-	-	-	-	0.02	-
c-C ₃ H ₂	0.03	0.36	0.21	0.04	0.27	-	-	-	0.03	0.07	0.07	0.19	0.26
C ₂ H	0.11	0.24	0.18	0.11	0.39	0.09	0.05	0.05	0.14	0.08	0.05	0.15	0.11
C ₂ D	-	0.05	0.05	0.04	0.05	-	-	-	-	-	-	0.06	-
CF ⁺	0.01	0.02	0.02	-	0.02	0.02	0.01	-	-	-	-	-	-
CH ₃ CCH	0.02	0.39	0.25	0.07	0.37	-	-	-	-	0.03	0.26	0.29	-
CH ₃ CN	-	0.93	0.08	-	0.08	-	-	-	-	1.27	0.10	-	-
CH ₃ OH	0.28	3.38	0.49	0.25	14.13	0.05	0.03	0.03	0.05	0.08	1.61	6.32	0.05
CN	0.41	0.62	0.48	0.20	0.33	0.48	0.13	0.09	0.11	0.44	0.31	0.91	0.40
¹³ CN	-	0.02	0.02	-	0.09	-	-	-	-	-	-	0.03	-
CS	0.31	0.03	0.43	0.04	0.05	0.07	0.03	0.02	0.02	0.25	0.37	0.02	0.27
¹³ CS	0.02	0.25	0.10	-	0.20	-	-	-	-	-	0.07	0.04	0.06
C ³⁴ S	0.02	0.10	0.10	-	<0.01	-	-	-	0.02	0.02	0.03	0.02	0.26
C ³³ S	-	0.10	0.02	-	0.09	-	-	-	-	-	0.03	0.02	0.03
HC ₃ N	-	0.75	0.19	-	0.32	-	-	-	-	-	0.32	0.07	0.03
HCN	0.08	0.01	0.01	0.18	<0.01	0.02	0.07	0.07	0.03	0.07	0.13	0.01	<0.01
DCN	0.11	0.06	0.08	0.02	0.08	-	-	-	-	0.06	0.04	0.02	0.04
H ¹³ CN	0.02	0.14	0.06	0.02	0.07	-	-	-	0.01	0.05	0.05	0.16	0.03
HC ¹⁵ N	-	0.36	0.05	-	0.05	-	-	-	-	-	0.03	0.02	-
HCO	-	0.01	0.01	-	0.04	-	-	-	-	-	-	0.02	0.04
HCO ⁺	0.18	0.03	0.01	0.09	0.03	0.34	0.04	0.30	0.03	0.09	0.32	0.07	0.58
DCO ⁺	0.01	0.04	0.04	0.02	0.07	0.01	0.01	0.01	-	-	-	0.02	-
H ¹³ CO ⁺	0.03	0.03	0.02	0.02	0.09	0.01	0.01	0.01	0.01	0.08	0.16	<0.01	0.03
HC ¹⁸ O ⁺	-	0.02	0.02	-	0.02	-	-	-	-	-	0.02	0.02	-
HC ¹⁷ O ⁺	-	-	-	-	-	-	-	-	-	-	-	-	-
HCS ⁺	0.01	0.11	0.11	-	0.14	-	-	-	-	0.02	0.05	0.03	-
HDO	-	0.03	-	-	-	-	-	-	-	-	-	-	-
H ₂ CCO	-	0.06	-	-	-	-	-	-	-	-	-	0.03	-
H ₂ CO	0.64	0.97	1.41	0.47	1.06	0.35	0.33	0.24	0.14	0.42	0.59	0.16	1.13
HD ₂ CO	-	0.11	0.02	0.02	0.10	-	-	-	-	-	0.02	0.06	-
H ₂ ¹³ CO	-	0.10	0.02	0.02	0.08	-	-	-	-	-	0.05	0.02	-
H ₂ CS	0.08	0.85	0.76	-	1.09	-	-	-	0.03	0.12	0.42	0.27	0.02
HD ₂ CS	-	-	-	-	0.03	-	-	-	-	-	-	0.04	-
H ₂ C ³⁴ S	-	-	-	-	-	-	-	-	-	-	-	-	-
H ₂ S	-	0.15	-	-	0.04	-	-	-	-	-	-	-	-
HNC	0.02	0.06	<0.01	0.03	0.02	0.08	0.08	0.02	0.02	0.09	0.03	0.03	0.03
DNC	0.01	0.10	0.02	0.02	0.07	-	0.01	-	-	-	-	0.02	-
HN ¹³ C	-	0.09	0.13	0.02	0.08	-	0.01	-	-	-	0.02	0.02	-
HNCO	-	0.11	-	-	0.03	-	-	-	-	-	-	-	-
N ₂ H ⁺	0.11	0.29	0.32	0.11	0.14	0.06	0.08	0.08	0.03	0.01	0.20	0.16	-
N ₂ D ⁺	-	0.01	0.01	0.03	-	-	-	-	-	-	-	-	-
NO	0.01	0.05	0.05	0.05	0.08	0.01	0.03	0.03	-	-	0.05	-	-
NS	-	0.19	0.18	-	0.18	-	-	-	-	-	-	0.13	-
OCS	-	0.35	-	-	-	-	-	-	-	-	0.10	-	-
SiO	0.08	0.35	0.30	-	0.26	-	-	-	-	-	0.54	-	-
²⁹ SiO	-	0.06	-	-	-	-	-	-	-	-	-	-	-
³⁰ SiO	-	-	-	-	-	-	-	-	-	-	-	-	-
SO	0.30	1.04	0.84	0.17	1.00	0.14	0.07	0.05	0.09	0.18	1.20	0.14	0.18
³⁴ SO	-	0.81	-	-	0.06	-	-	-	-	-	0.04	0.01	-
SO ⁺	-	-	-	-	0.05	-	-	-	-	-	-	0.02	0.04
SO ₂	0.07	4.28	0.16	-	0.38	-	-	-	-	-	1.48	-	-

Notes. Errors refer to the Gaussian line fits and do not account for the calibration uncertainties discussed in Section 2.2. Errors add up for species with many transitions and are usually larger in cases of strong overlap between lines. However, they are generally 2% – 6%.

Table A.3: Overlap between regions. To be read from left to right, e.g. $\sim 39\%$ of the ‘high column density’ region overlaps with the ‘low temperature’ region. Conversely, $\sim 9\%$ of the ‘low temperature’ region overlaps with the ‘high column density’ region.

	high column density	high column density without KL and Orion South	high column density, low temperature	high column density, high temperature, without KL and Orion South	low column density	low temperature	low column density, low temperature	low column density, high temperature	high temperature without KL and Orion South	H II	radical region	dense PDR
high column density	-	0.924	0.393	0.494	-	0.393	-	-	0.494	0.085	0.159	-
high column density without KL and Orion South	1.000	-	0.426	0.535	-	0.426	-	-	0.535	0.063	0.172	-
high column density, low temperature	1.000	1.000	-	-	-	1.000	-	-	-	-	-	-
high column density, high temperature, without KL and Orion South	1.000	1.000	-	-	-	-	-	-	1.000	0.086	0.321	-
low column density	-	-	-	-	-	0.498	0.498	0.502	0.502	0.024	0.008	0.025
low temperature	0.090	0.090	0.090	-	0.910	-	0.910	-	-	-	-	-
low column density, low temperature	-	-	-	-	1.000	1.000	-	-	-	-	-	-
low column density, high temperature	-	-	-	-	1.000	-	-	-	1.000	0.047	0.015	0.050
high temperature without KL and Orion South	0.109	0.109	-	0.109	0.891	-	-	0.891	-	0.051	0.049	0.045
H II	0.311	0.211	-	0.156	0.689	-	-	0.689	0.844	-	-	0.256
radical region	0.722	0.722	-	0.722	0.278	-	-	0.278	1.000	-	-	-
dense PDR	-	-	-	-	1.000	-	-	1.000	1.000	0.348	-	-

Notes. The majority of these overlaps are discussed in this paper as they correspond to regions themselves (e.g. the overlap between the ‘high column density’ and ‘low temperature’ regions is identical to the region ‘high column density, low temperature’). The exceptions to this are the three regions that are not based on column density or temperature thresholds, namely ‘H II’, ‘radical region’, and ‘dense PDR’.

Appendix B: Additional figures

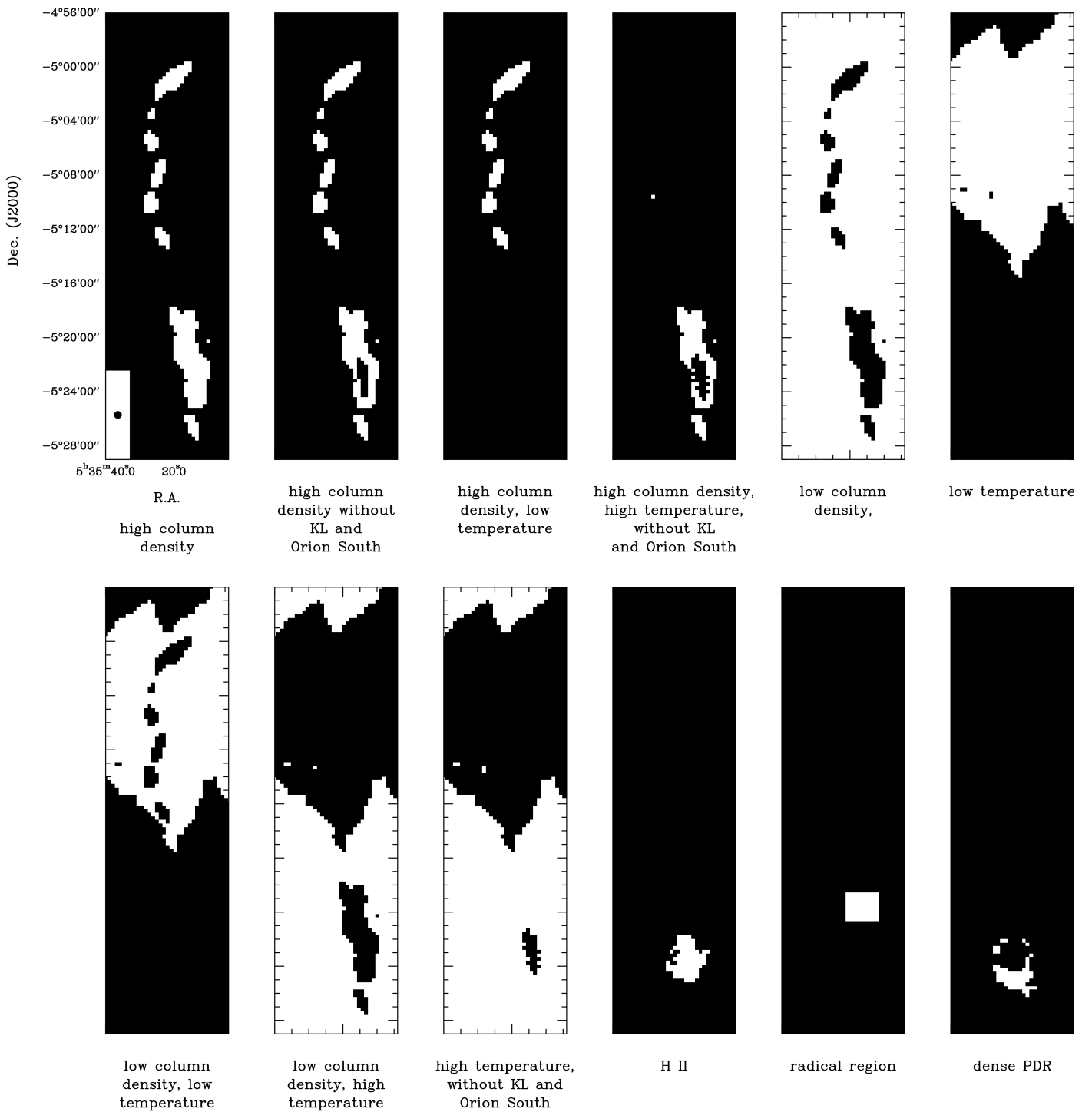
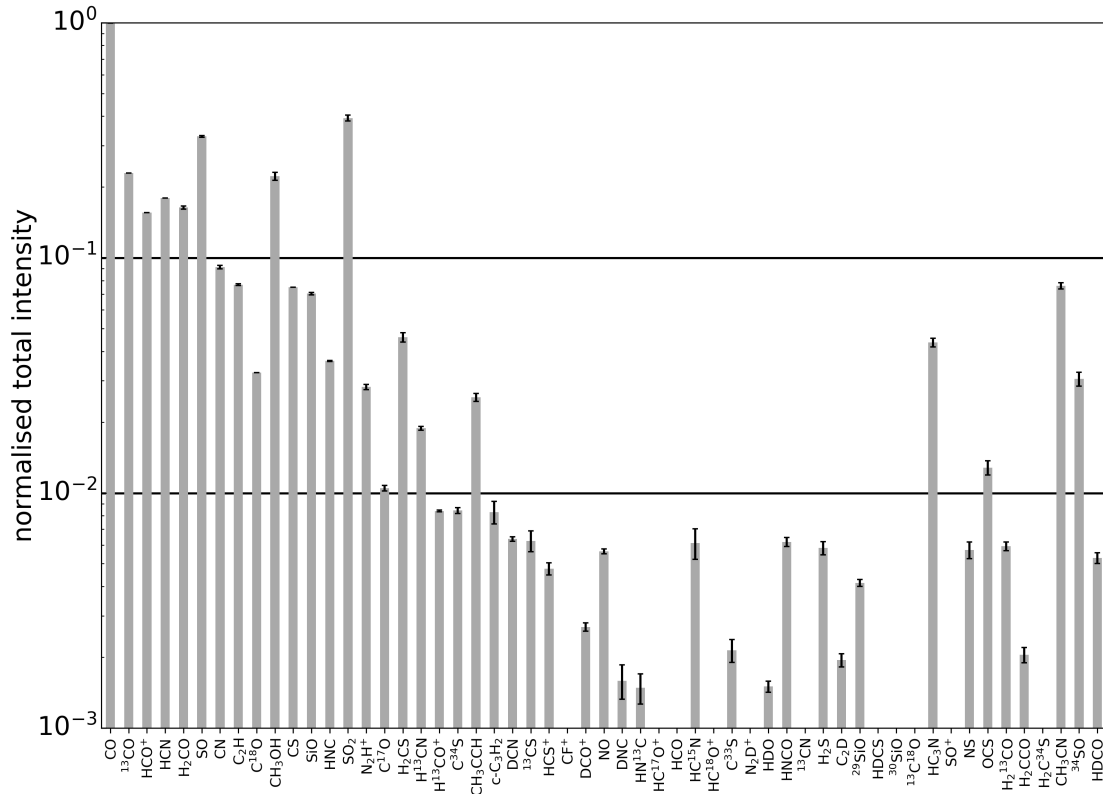
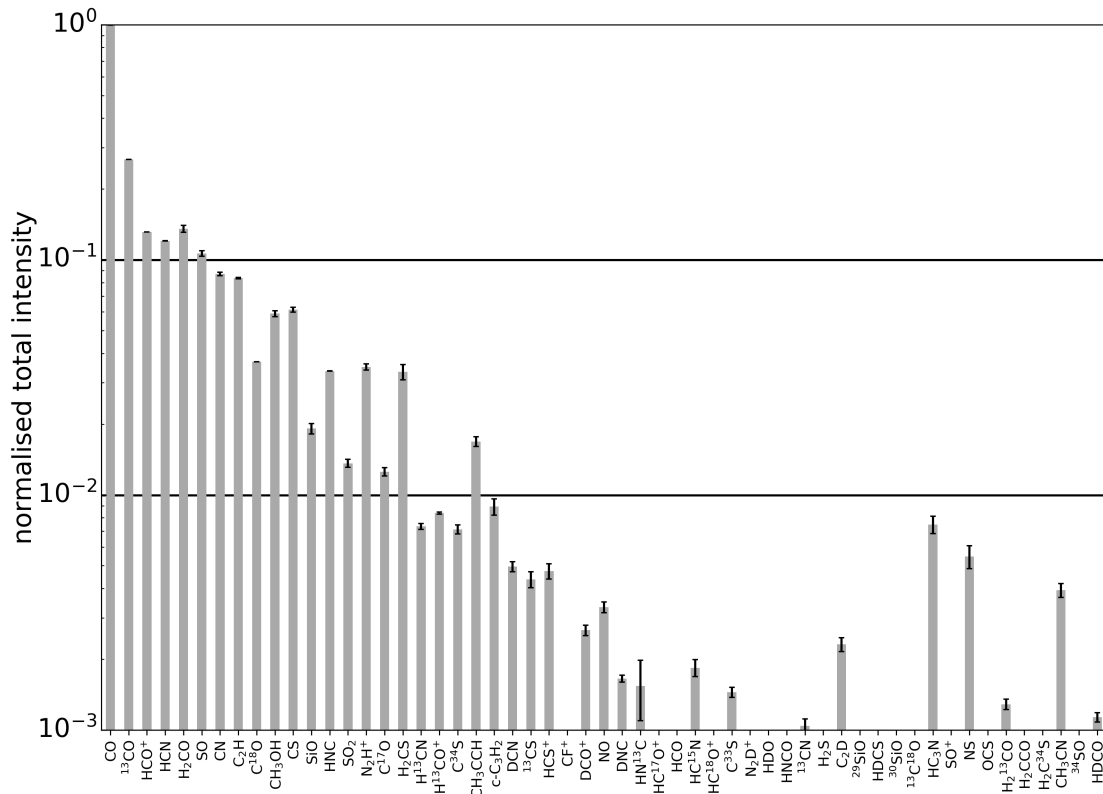


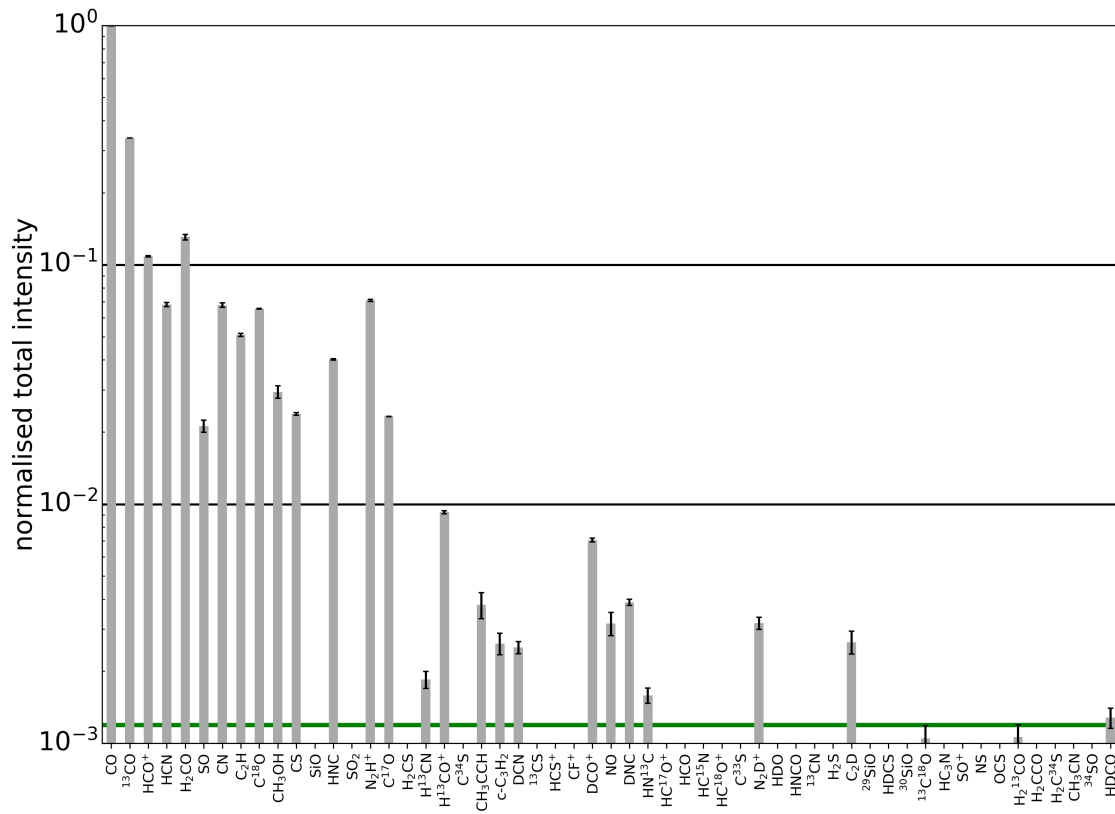
Fig. B.1: Masks obtained with the parameters listed in Table 3. The images are intended as a visual aid and give an impression of the spatial extension of the considered regions. White pixels are part of the region, black pixels are not.



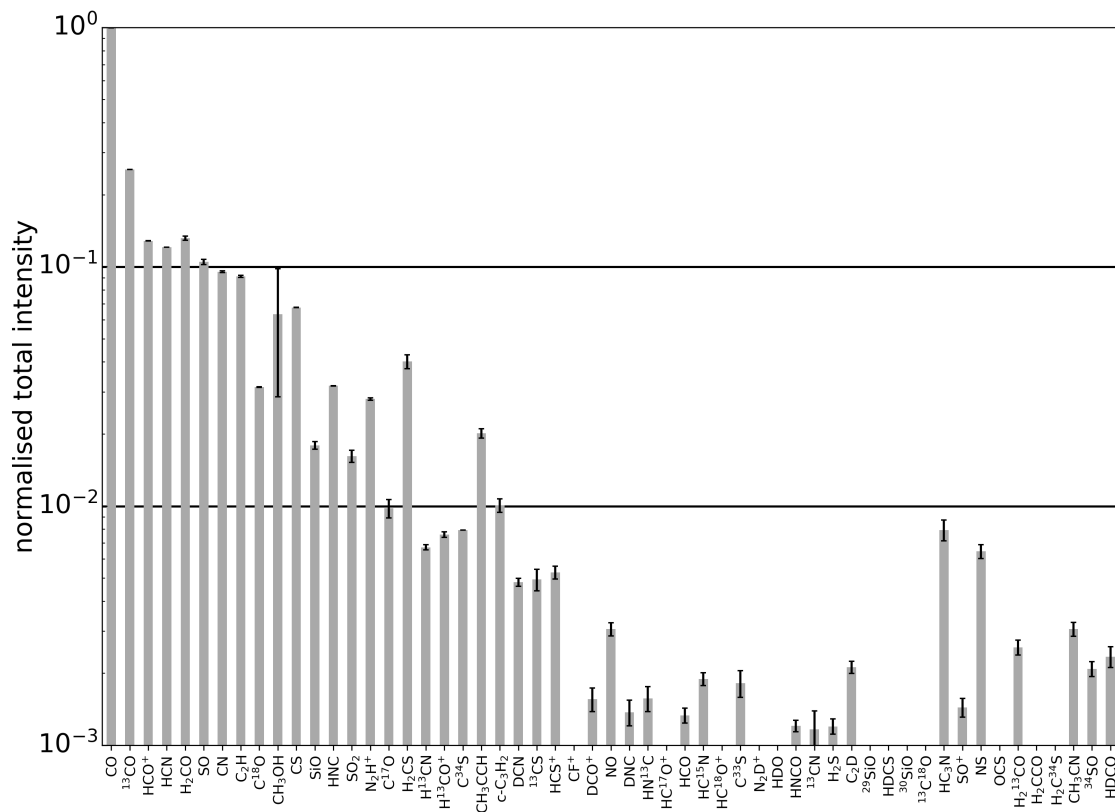
(a) high column density



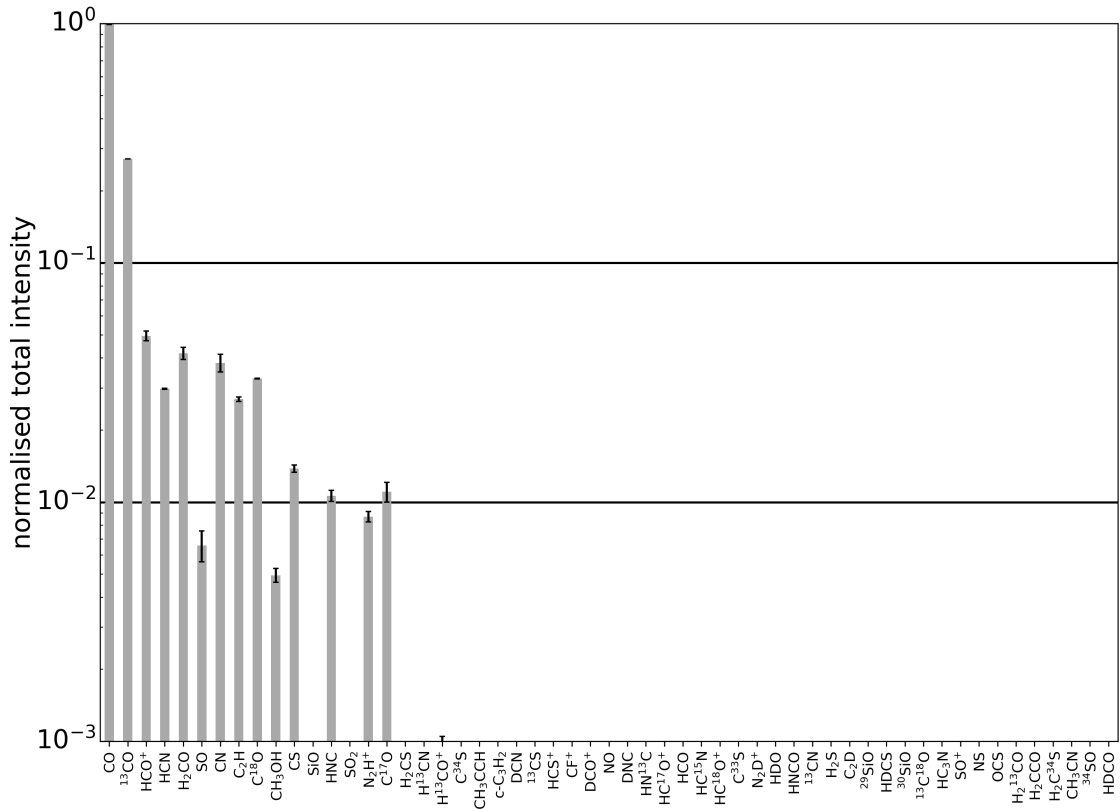
(b) high column density, without KL and Orion South



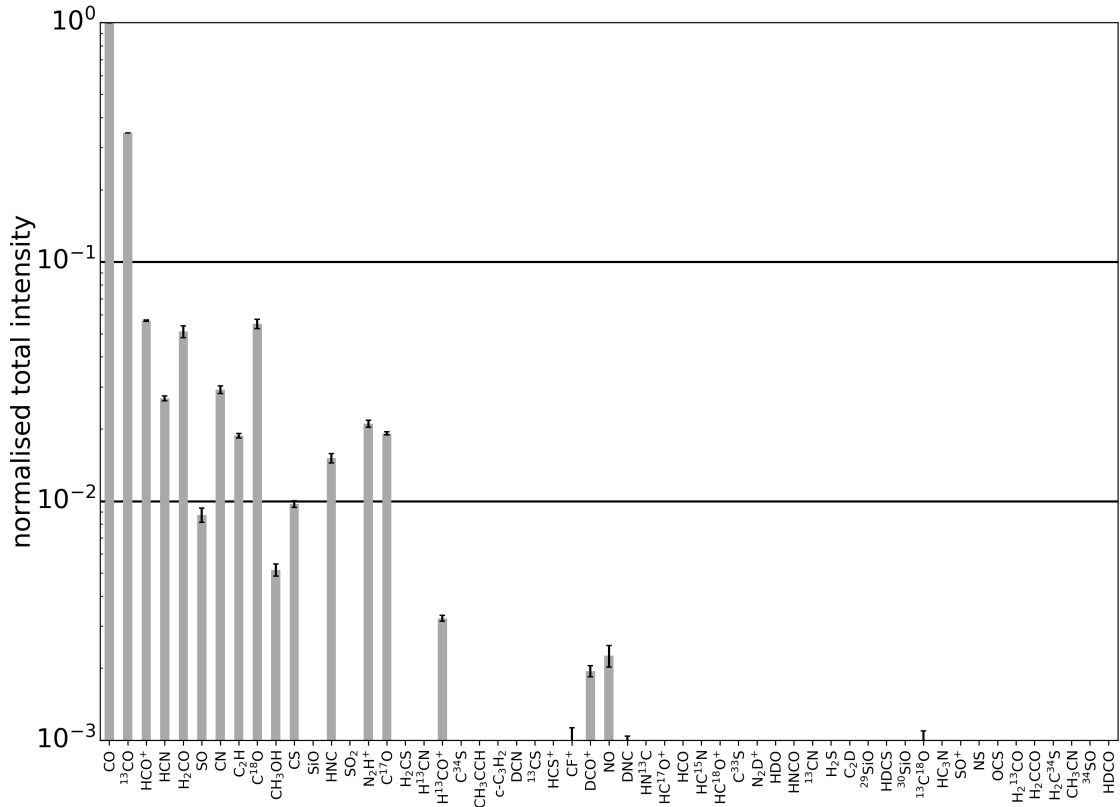
(c) high column density, low temperature



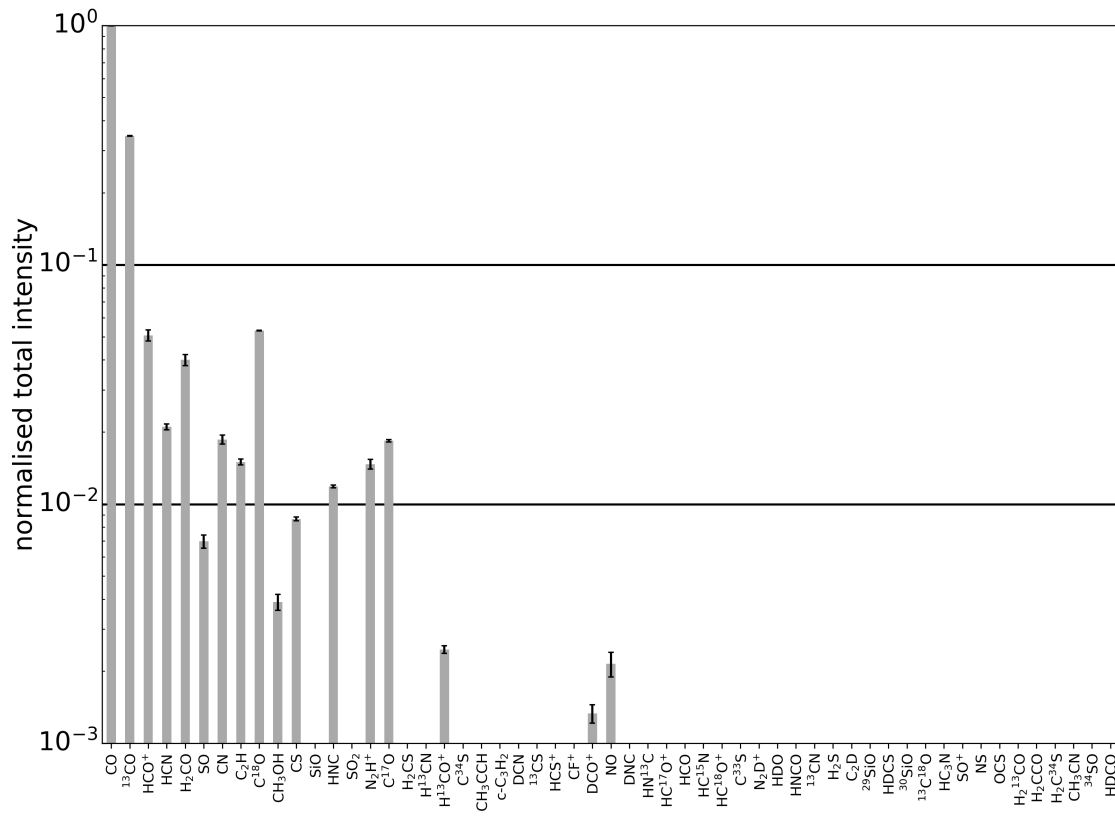
(d) high column density, high temperature, without KL and Orion South



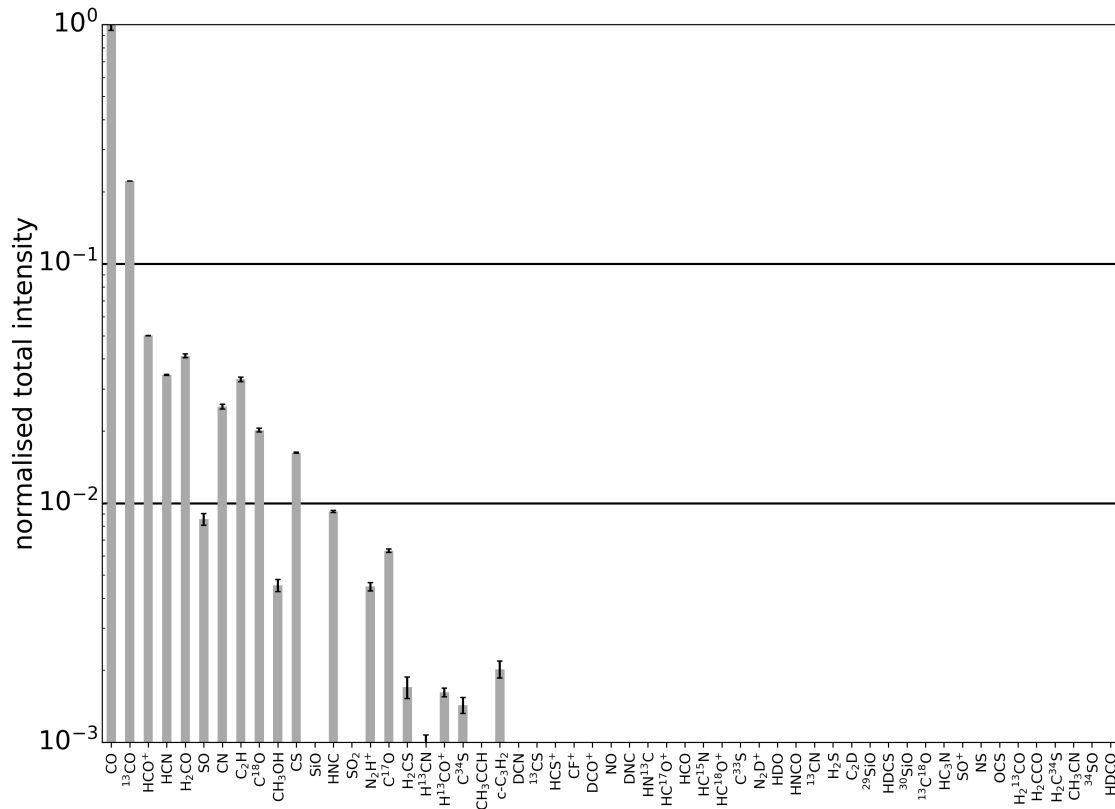
(e) low column density



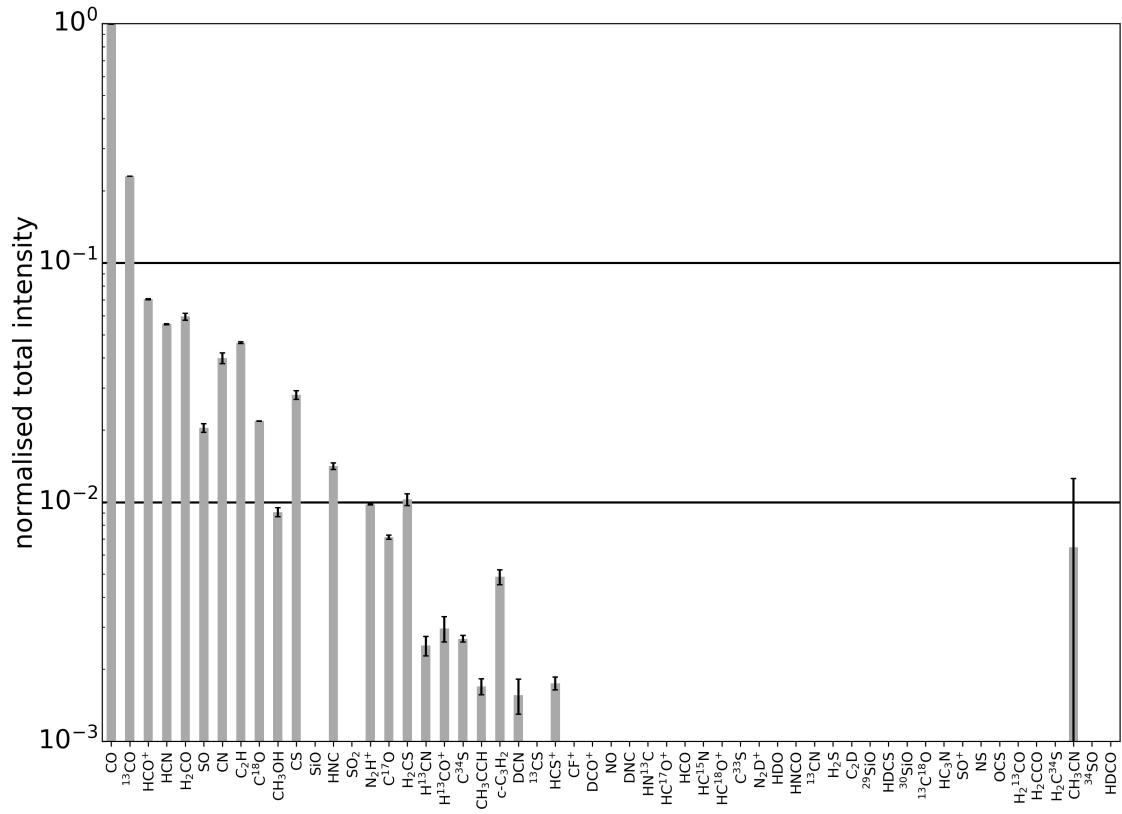
(f) low temperature



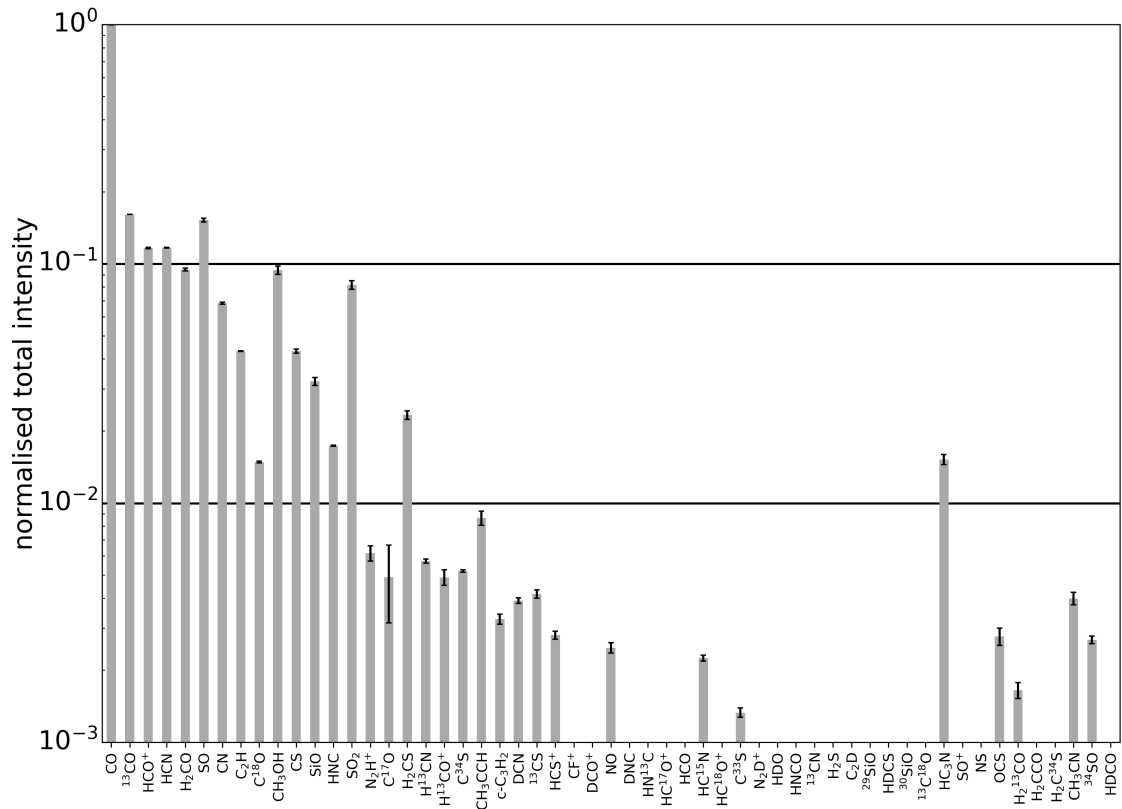
(g) low column density, low temperature



(h) low column density, high temperature



(i) high temperature, without KL and Orion South



(j) H II

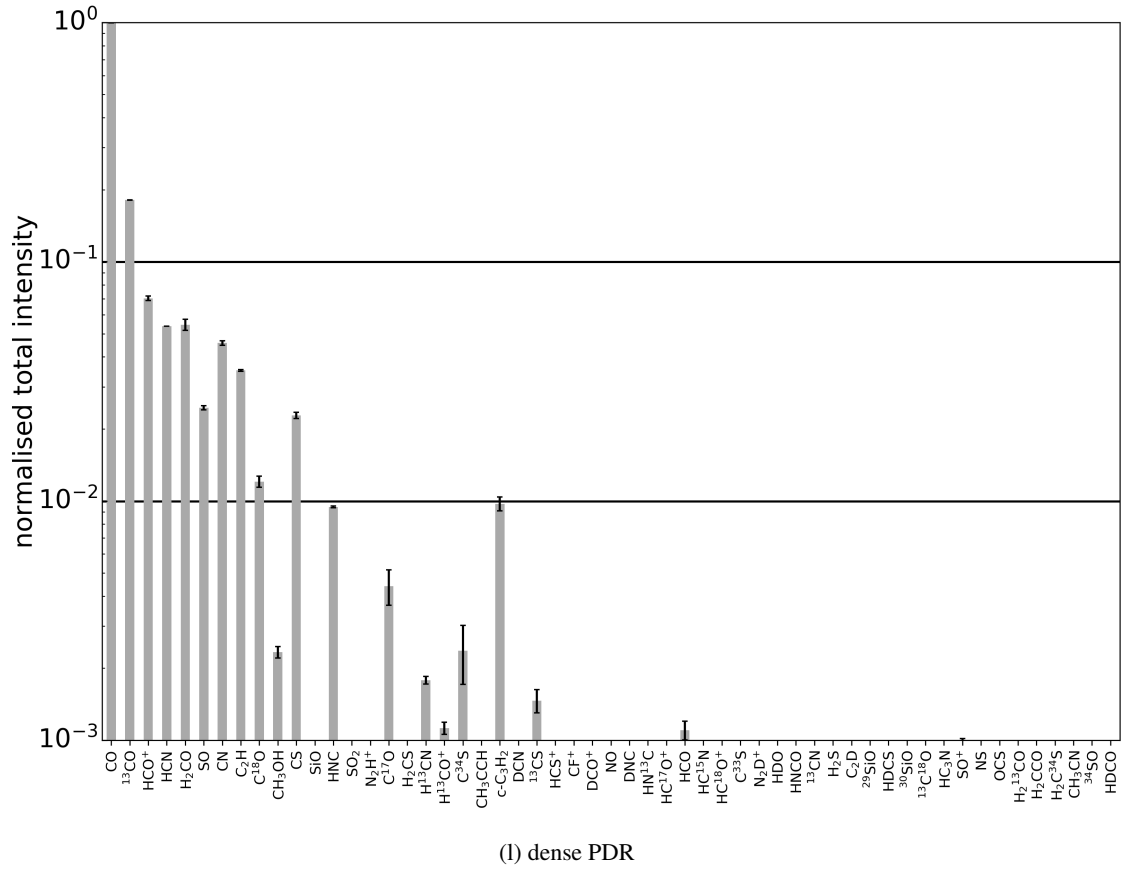
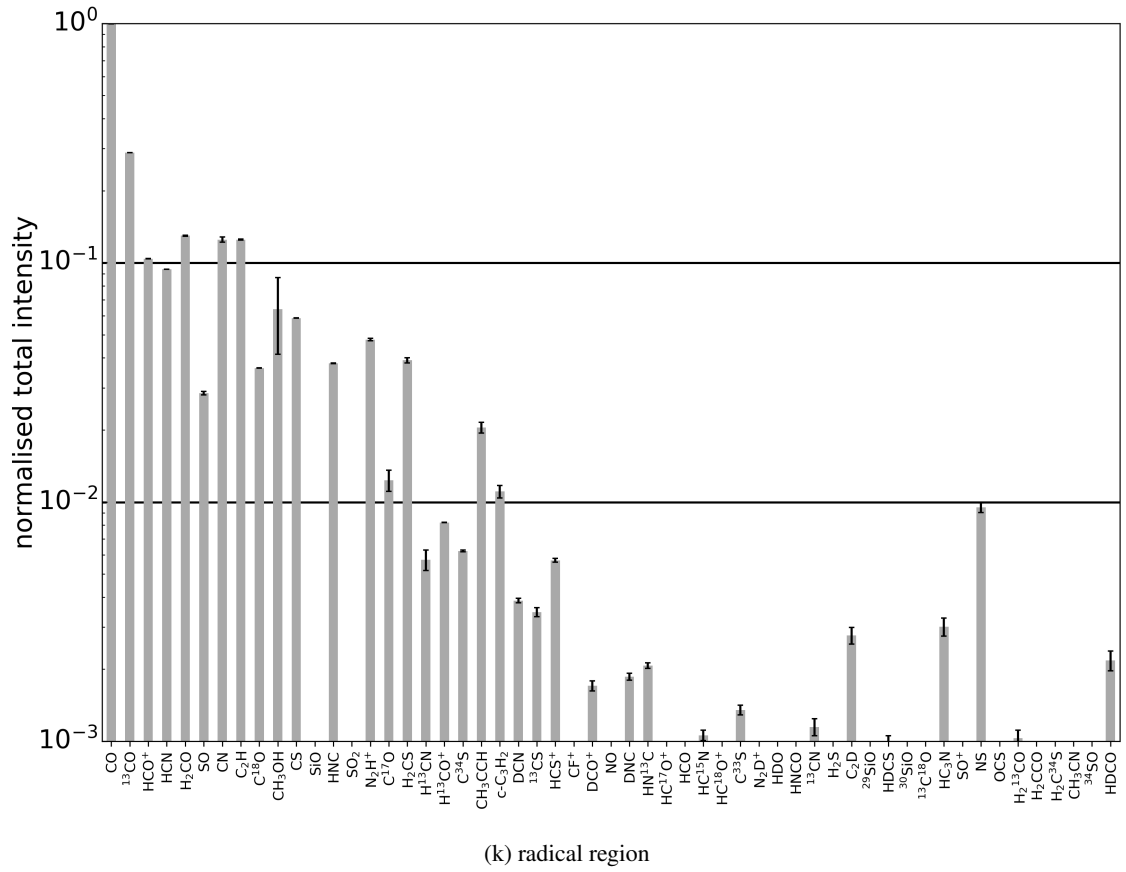


Fig. B.2: Total intensities of all considered species for the regions described in Table 3, normalised by the respective total CO intensity. Due to the noise level of the region and its total CO intensity, a normalised total intensity of 0.1% is not detectable for region (c). Therefore, a green line approximating the detection limit for a 5σ feature (assuming the median line width of the region and σ_{median}) is added in this case. Detections below that limit indicate that the local noise is below σ_{median} . Error bars refer to the fit uncertainties.

Percentage of the total intensity emitted by the different species

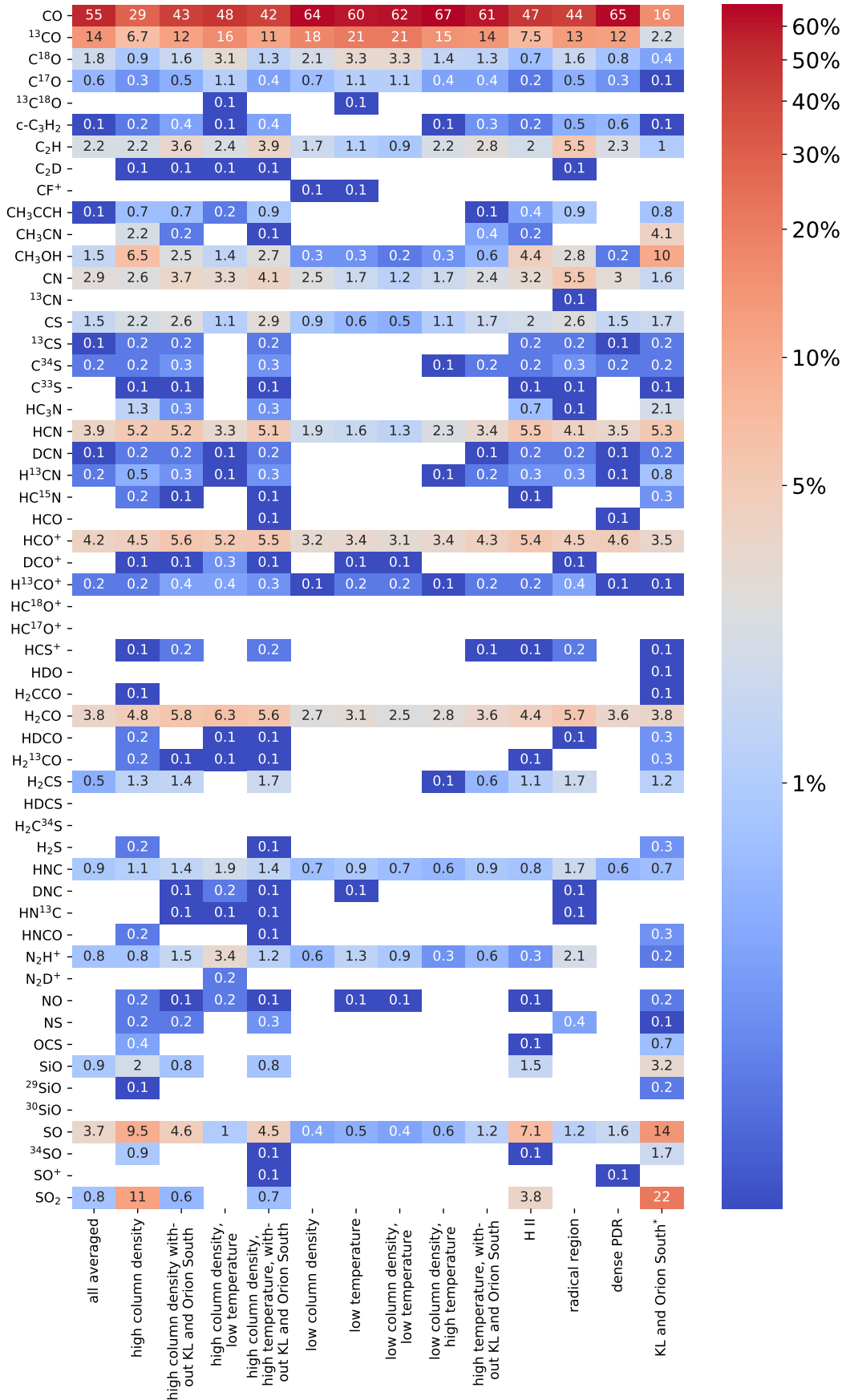


Fig. B.3: Share of each species to the total intensity of each region. For each species (rows), the colour bar offers a visual aid to quickly identify regions with lower or higher values. For each region (columns), the colour bar helps to assess the influence of different species. Shares under 0.1% are blank. (*) The values for ‘KL and Orion South’ are approximated as discussed in Section 4.1.

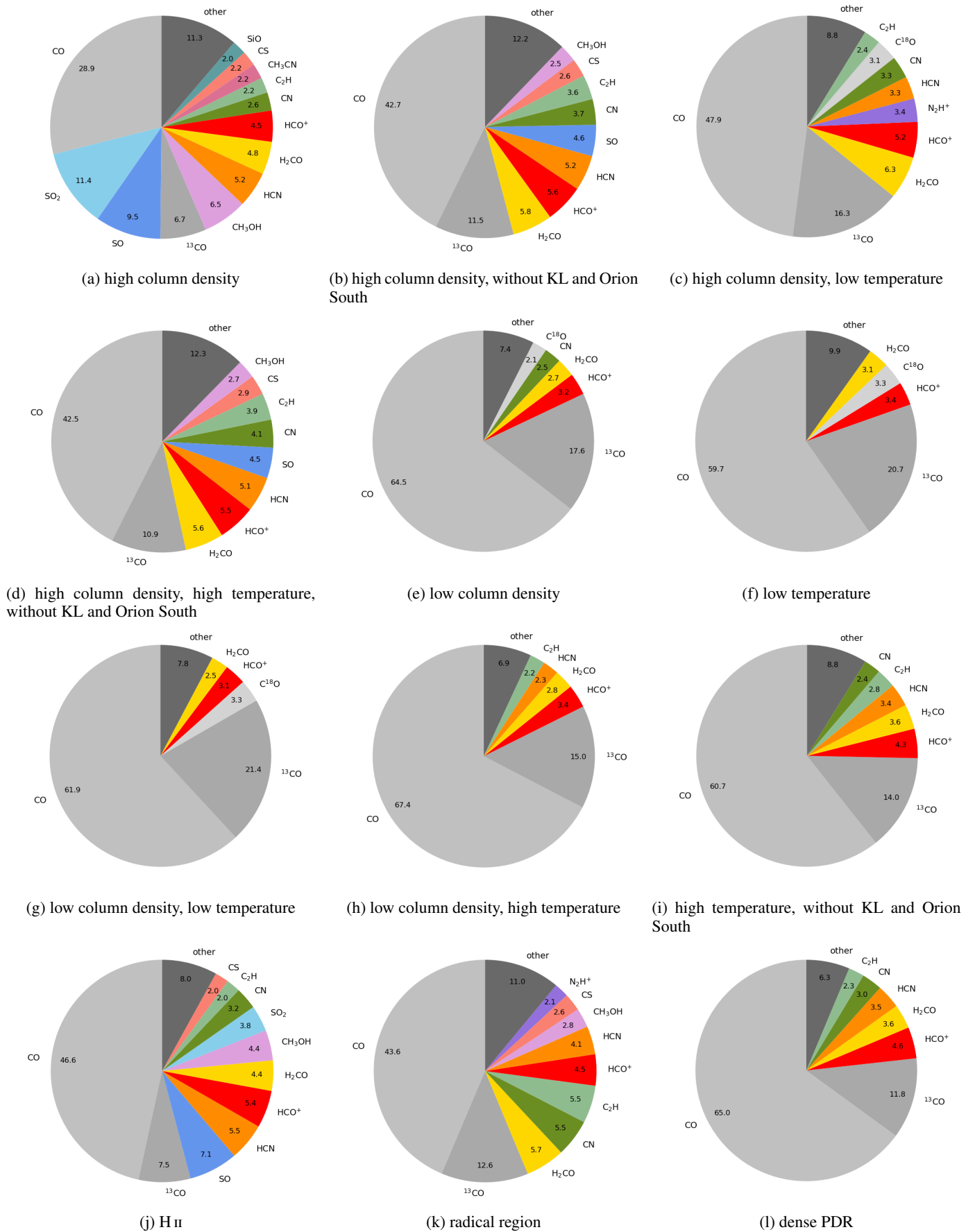


Fig. B.4: Pie charts depicting the share of the total intensity emitted by different species for all regions from Table 3 (see Fig. 5 for the plot of the averaged data). Shares under 2% are summed under ‘other’.

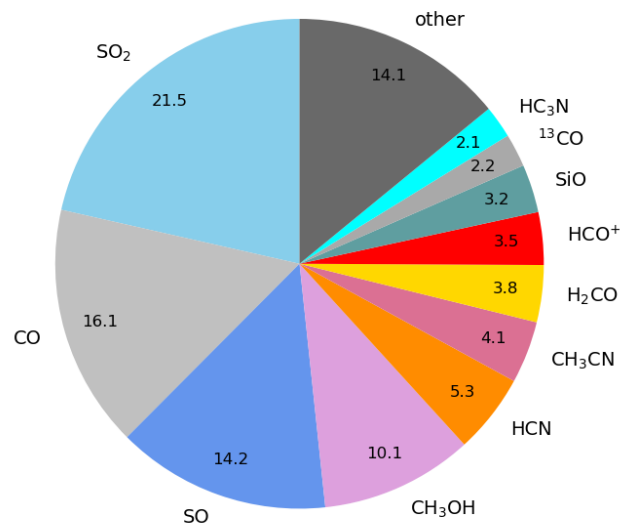


Fig. B.5: Approximated emission profile from the region around KL and Orion South.

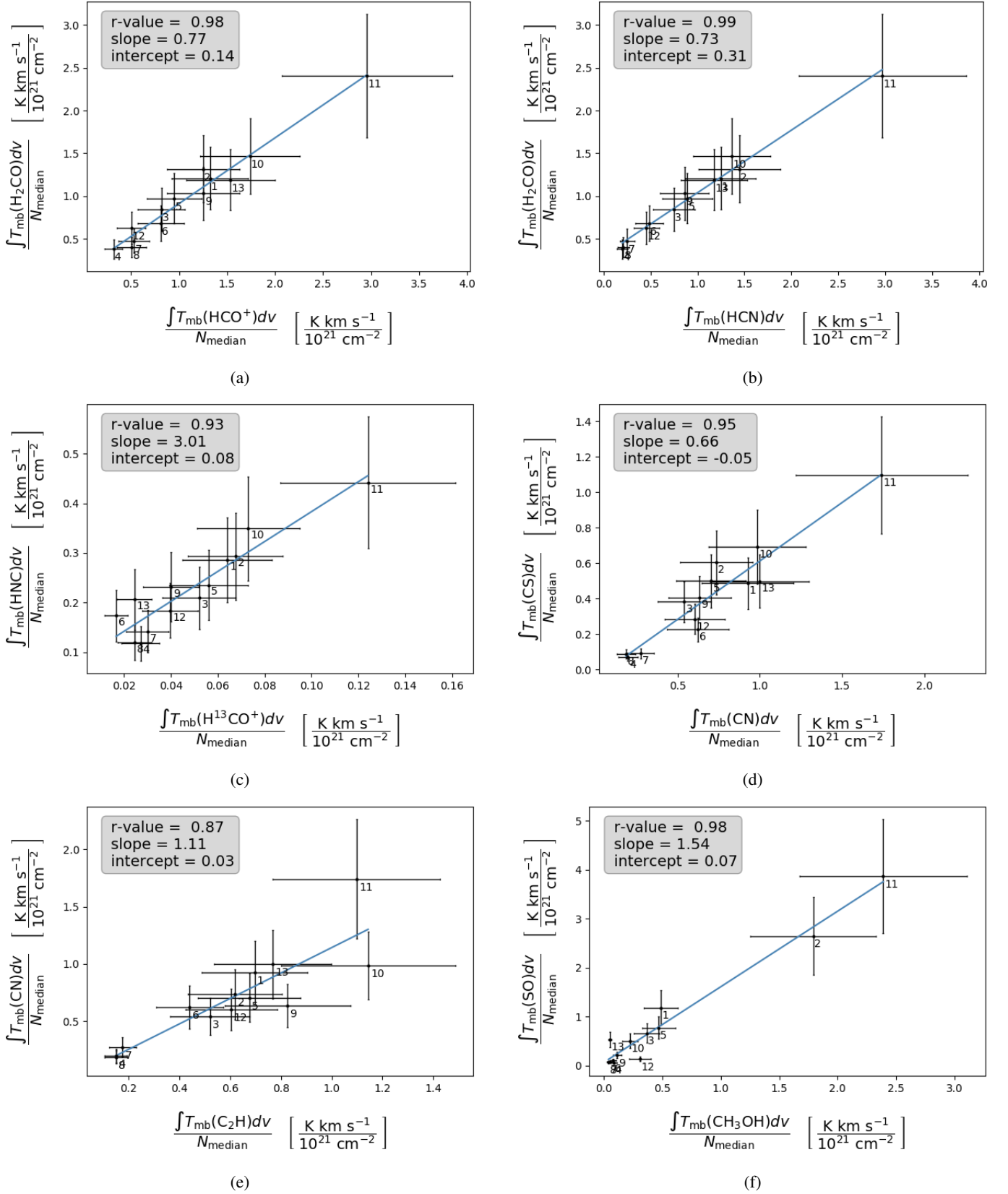


Fig. B.6: Examples of correlation plots between species. The numbers refer to the region identifiers listed in Table 3. Due to the small number of samples, the r -value should be viewed with caution; it only gives an indication of possible correlation. The error bars indicate the assumed 30% uncertainty.

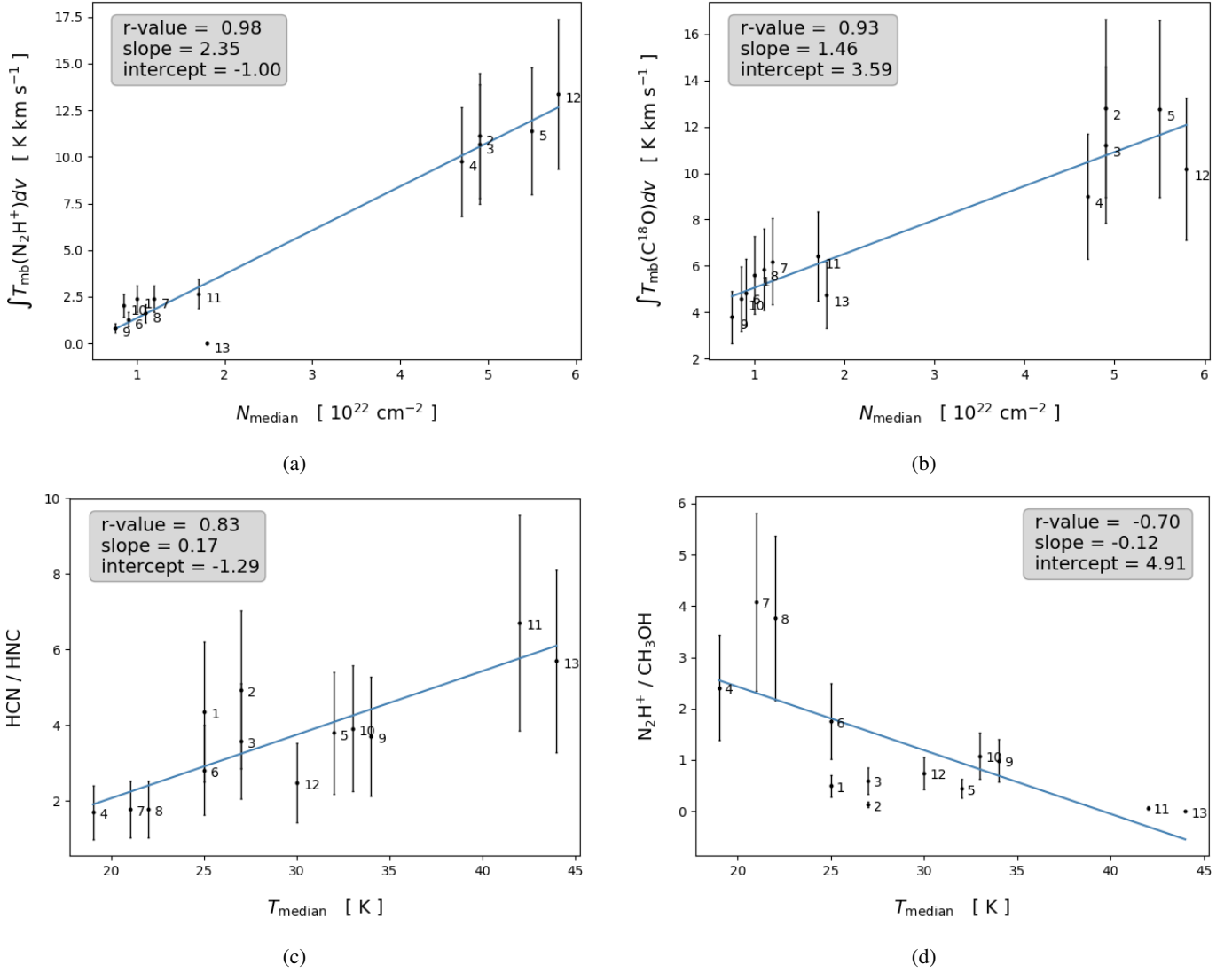


Fig. B.7: Examples of correlation plots between species and physical parameters. The numbers refer to the region identifiers listed in Table 3. Due to the small number of samples, the r-value should be viewed with caution; it only gives an indication of possible correlation. The error bars indicate the assumed 30% uncertainty.